國 立 交 通 大 學
顯示科技研究所

碩士論文

非晶矽 / 微晶矽 疊層薄膜太陽能電池之模擬與微晶矽結晶率之探討

Tandem a-Si:H / μc-Si:H Thin Film Solar Cells: Modeling & Control of Crystallinity of μc-Si:H

研究生：曾威豪 Wei-Hao Tseng
指導教授：蔡娟娟 教授 Prof. C.C Tsai

中華民國九十八年 八月

非晶矽 / 微晶矽 疊層薄膜太陽能電池之

模擬與微晶矽結晶率之探討

Tandem a-Si:H / μc-Si:H Thin Film Solar Cells:

Modeling & Control of Crystallinity of μc-Si:H

研究生 ： 曾威豪 Student: Wei-hao Tseng

指導教授 ： 蔡娟娟 教授 Advisor: Prof. C.C. Tsai

國立交通大學

顯示科技研究所

碩士論文

A thesis

Submitted to Department of Photonics

Display Institute

College of Electrical Engineering and Computer Science

National Chiao Tung University

In partial Fulfillment of the Requirements

For the Degree of

Master

In

Electro-Optical Engineering

August 2009

Hsinchu, Taiwan, Republic of China

中華民國九十八年八月

中文摘要

在本論文中，我們以 Atlas 軟體建立新型矽基薄膜太陽電池模擬模組，並討論各種物理參數對於元件效率的影響。單接面的氫化非晶矽和氫化微晶矽太陽能電池皆以 Atlas 模擬出其電學特性，之後再將非晶矽和微晶矽電池疊層構成的雙接面太陽能電池進行模擬。當改變底層太陽能電池吸收層的能隙以及電子能態中帶尾能態的分佈時，開路電壓 (V_{oc}) 會隨著能隙增加而上升，短路電流 (J_{sc}) 則是在能隙小於 1.4 電子伏特後，開始下降。這是因爲電子和電洞佔據在侷限能態 (localized state) 上是無法有效移動，造成短路電流 (Jsc) 的下降。除此之外，我們也利用射頻電漿輔助化學氣相沉積系統 (PECVD) 製作氫化微晶矽薄膜。對於氫化微晶矽薄膜太陽能電池而言，結晶率是相當重要的議題。實驗中以利用調變氫氣流量，電漿能量還有不同的基板進行對於控制結晶率的研究。

Abstract

In this study, a detailed electrical-optical computer modeling, based on the Atlas software, was used to investigate the effect of bandgap (E_g) and tail state distribution of intrinsic microcrystalline silicon thin film on thin film silicon solar cells. Complete tandem solar cell which consists of an a-Si:H top cell and a μc-Si:H bottom cell solar cell were simulated. In this study the bandgap and tail state distribution of the bottom cell were varied. The acceptor and donor tail state distribution of i-layer was assumed to be broader as the E_g increases in the bottom cells. WTA and WTD are used to represent the characteristic energy for acceptor-like tail state distribution, and characteristic energy for the donor-like tail state distribution, respectively. The open circuit voltage (V_{oc}) increased with increasing E_g, but the short circuit current (J_{sc}) decreases when E_g is lower than 1.4eV. The lower E_g made the V_{oc} and efficiency decease sharply, although the J_{sc} was kept at high value. Comparing the highest (1.6 eV) and lowest E_g (1.1 eV), the former has a better performance. Therefore, the E_g of bottom cell should not be lower than 1.3eV to avoid the decline of efficiency.

In the second part of this thesis, I have studied the control of crystallinity in the growth

of μc-Si:H thin films during plasma-enhanced chemical vapor deposition (PECVD) process. The crystallinity of μc-Si:H film increases with increasing film thickness. Through modulating the H_2 flow in the deposition process, the crystallinity could be controlled. Base on the experimental results, the initial deposition condition is crucial for further growth. Through altering the deposition conditions and modulating the hydrogen flow, uniform crystallinity of about 50% could be achieved.

誌謝

兩年以來，從一個完全不懂太陽電池的學生到現在順利完成論文，真的要感謝許多曾幫過我的人，首先必須要感謝顯示所的冉曉雯副教授，在實驗研究部份因為有老師的細心指導還有在旁的協助，才能使我的研究能得以順利進行，在此特別感謝老師的栽培以及付出。接下來我的指導教授蔡娟娟老師，她教導我許多做人處事方法以及研究學問的態度，在這兩年研究生涯的敦敦教誨之下使我受益匪淺。在科學研究方面的嚴謹態度，在社會上做事的方式，使得學生在兩年碩士生涯學習甚多，特此感謝老師的指導。

還要感謝綠色能源研究中心在實驗上給我的各種幫忙，口試委員冉曉雯老師、吳耀銓老師、劉柏村老師於百忙之中撥冗前來，提供我許多寶貴意見，使得本論文更臻於完善。此外，交通大學奈米中心的林聖欽先生、倪月珍小姐、黃國華先生、何惟梅小姐、崔秉鉞主任、優貝克的陳江耀、張文心、張智浩及Morris在裝機時以及實驗上的指導還有Silvaco的范萬達，各位在這裡給我的各種幫忙，內心亦不勝感激。

感謝博後光電所博士班顏國錫學長、黃彥棠學長、徐振航學長、光電所王建敏同學、顯示所姚芳弘、陳達欣同學，同學之間的互相勉勵以及另外一組的黃慶能、袁煥之大家感情融洽，常常忙裡偷閒，使得兩年的碩士生涯充滿了回憶，還有許翼鵬、許宏榮、李建亞、鄭柏翔學弟以及另一組的琇文學妹和世益學弟大家給予我的實在太多太多，除了協助實驗之外並在我最艱苦的時候陪我渡過最後的關頭，所有在本實驗室的碩一學弟妹，看到你們所製作的卡片，真的讓我很感動，謝謝大家，在此獻上我最誠摯的祝福與

謝意。最後，要深深感謝我最愛的家人，陪我度過許多挫折及分享我的喜悅，並在精神上永遠支持我，沒有你們在背後的支持就沒有現在的我，在此，願將這份榮耀與你們一同分享。

Contents

Figure Captions

Chapter 1

Chapter 2

Chapter 3

Chapter 4

Table Captions

Chapter 4

Chapter 1

Introduction

1.1 Current Progress of Solar Cell Technologies

The constant energy consumption and expansion of population add to the potential risks of ecological and human disaster associated with global warming. This makes the energy crisis will be the top issue affecting the humanity 50 years from now. It is necessary to develop renewable energy technologies such as photovoltaic energy. These technologies already exist, however, the cost disadvantage of the PV is still significant compared to fossil-based and nuclear energies, despite of the variety of PV technologies. There are many different types of PV design using different type of materials or structures as shown in **Fig.** . For the common crystalline and multi-crystalline silicon cells which have high conversion efficiencies, there are the III-V and the chalcopyrite based solar cells composed of more exotic compounds (As, Sb, Ga, In,...) which have also high conversion efficiencies. But these technologies cause serious contamination for global environment because of the toxicity of their constituents. All these types of cells can be combined into multi-junction cells which present very high conversion efficiencies of up to 30 %. The main disadvantage of these cells is that they are all deposited on crystalline silicon wafers making them economically and environmentally expensive. On the other hand, chemical dye sensitized cells are very cheap, but show poor conversion efficiency of about 5 - 7 % [1] so far.

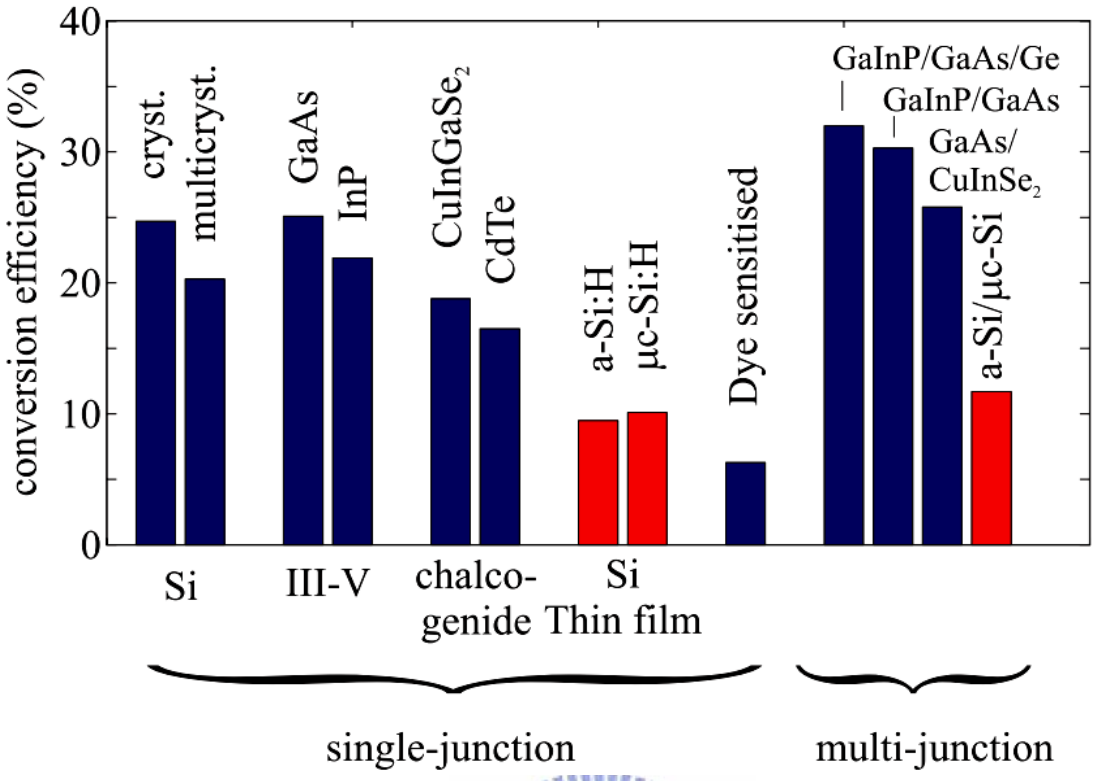

Fig. 1-1 Panel of the different PV technologies with their conversion efficiencies, from high performance multi-junction GaInP/GaAs/Ge to very low cost chemical dye sensitized cells [13].

1.2 Silicon Thin Film Solar Cell

The silicon thin film does not come from expensive monocrystalline ingots but is grown by chemical vapor deposition (CVD) on inexpensive substrates such as glass, stainless steel or plastic. The deposited silicon can present as either an amorphous (a-Si:H) or a microcrystalline (µc-Si:H) structure and the resulting PV solar cells with conversion efficiency of about 10% can be achieved [13].

Hydrogenated amorphous silicon (a-Si:H) is the non-crystalline allotropic form of silicon. It can be deposited in thin films at low temperatures onto a variety of substrates. Silicon is a four-fold coordinated atom that is normally tetrahedrally bonded to four neighboring silicon atoms. In crystalline silicon this tetrahedral structure is continued over a large range, forming a well-ordered lattice (crystalline), as shown in **Fig. 1-2(a)**. In amorphous silicon this long

range order is not present and the atoms form a continuous random network, as shown in **Fig. 1-2(b)**. Not all the atoms within amorphous silicon are four-fold coordinated. Due to the disordered nature of the material some atoms have a dangling bond. These dangling bonds are defects in the silicon random network, which cause anomalous electrical behavior. If desired, the material can be passivated by hydrogen, which bonds to the dangling bonds and can reduce the dangling bond density by several orders of magnitude. In general, there exist about 10 at% hydrogen concentrations in hydrogenated amorphous silicon thin film. Hydrogenated amorphous silicon has a sufficiently low amount of defects to be used within devices. However, the hydrogen is unfortunately associated with light induced degradation of the material, termed the Staebler-Wronski effect.

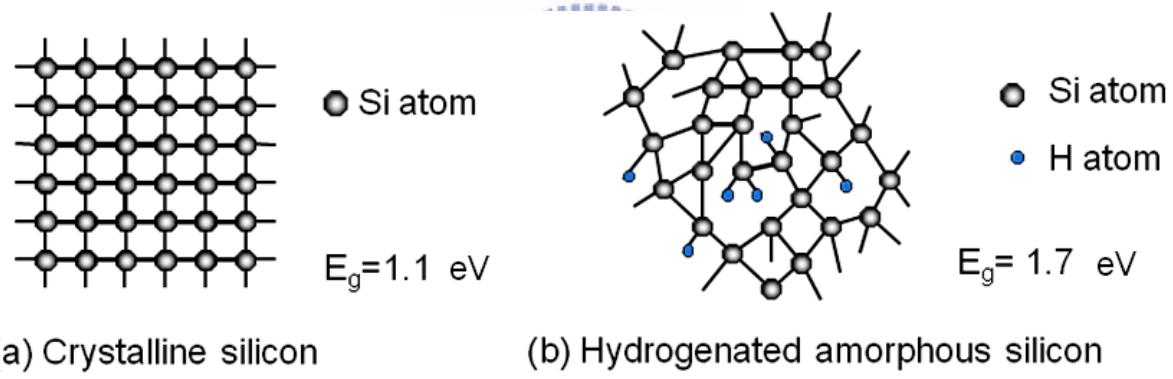

Fig. 1-2 Silicon atomic structure of (a) crystalline silicon (b) hydrogenated amorphous silicon.

Microcrystalline and amorphous silicon layers have quiet different material properties:

(1) It is a complex material microstructure that made by drastic deposition conditions.

(2) It is sensitivity to layer contamination.

(3) The bandgap of μc-Si:H is lower than a-Si:H (1.7 to 1.8 eV for a-Si:H). Due to this, the incoming light in the near infrared region of the solar spectrum can be absorbed.

(4) An indirect bandgap, it means a lower absorption coefficient in the visible range of the solar spectrum compared with a-Si:H. Therefore it is necessary for using thicker

absorbing layers than in the case of a-Si:H and more efficient light trapping within the solar cell.

(5) The most important thing is a much milder from the light induced degradation.

The best single junction microcrystalline silicon solar cells have 9 to 10 % range efficiency. Now the best way of using the microcrystalline silicon for photovotaics at present is the tandem solar cell which is the combination of these two materials into a multi-junction a-Si:H/μc-Si:H solar cell increases the conversion efficiency up to 11.7 % [1], but one hopes to reach an efficiency near 15 % [2]. The tandem thin film solar cells have many advantages compared to the other PV technologies, even if their conversion efficiency is lower than solar cells based on crystalline silicon or III-V compounds. First, it can be deposited on large area substrates, or it can be deposited continuously on flexible substrate in a roll-to-roll process. Second, the quantity of raw material used to produce a thin film solar cell is much lower than for ≈ 300 μm thick crystalline silicon wafers, since the total thickness of the deposited films is less than 10 μm. Therefore, thin film silicon solar cells are cheaper and the economical and energy pay-back times are shorter than for the other PV technologies.

1.3 Silvaco Device Simulator

Simulation of the optical and electrical behavior of semiconductor devices is an established method for improving existing devices, obtaining insight into their physical operation, and developing new devices. A number of sophisticated semiconductor device-simulation packages are already commercially available on the market such as Atlas from SILVACO Data Systems Inc [3]. ATLAS provides general capabilities for physically-based two (2D) and three-dimensional (3D) simulation of semiconductor devices. A wide variety of devices can be modeled inclusive of MOSFETs, BJTs, HRTs, power devices, photodetectors, LEDs and solar cells, with the most advanced physical models available.

Atlas allows device design to be optimized for best performance without fabrication, eliminating the need for costly experiments. It models the two dimensional distributions of potential and the carrier concentrations in the device. The primary function of Atlas is to solve numerically the following basic semiconductor device equations :

The Poisson's equation

$$\nabla \cdot \varepsilon \vec{E} = q\left(p - n + N_D^+ - N_A^- + N \right) \qquad \text{Eq. 1-1}$$

The total electron and the total hole current density equations in material :

$$\vec{J}_n = \vec{J}_n^{\,drift} + \vec{J}_n^{\,diff} = q\mu_n n\vec{E} + qD_n \nabla n = -q\mu_n n \nabla \varphi + qD_n \nabla n$$

$$\vec{J}_p = \vec{J}_p^{\,drift} + \vec{J}_p^{\,diff} = q\mu_p p\vec{E} - qD_p \nabla p = -q\mu_p p \nabla \varphi - qD_p \nabla p \qquad \text{Eq. 1-2}$$

The total current density :

$$\vec{J} = \vec{J}_p + \vec{J}_n \qquad \text{Eq. 1-3}$$

The electron and hole continuity equations :

$$\nabla \cdot \overrightarrow{J_n} = q(R_n - G + \frac{\partial n}{\partial t}) \qquad \text{Eq. 1-4}$$

$$\nabla \cdot \overrightarrow{J_p} = q(G - R_p - \frac{\partial p}{\partial t}) \qquad \text{Eq. 1-5}$$

ε is the dielectric permittivity, φ is the electrostatic potential, n and p are the electron and hole concentrations, N_D^+ and N_A^- are the ionized donor and acceptor impurity concentrations, N is the net charge exclusive of electron, hole, ionized donor, ionized acceptor which may be present due to the fixed charge insulating material or charge interface states. Simultaneous numerical resolution of the Poisson Equation (Eq. 1-1) obtains the electric field ($\vec{E}$) and the width of the depletion region. $\vec{J}_n$ and $\vec{J}_p$ are vectors of the electron and hole current density. μ_n and μ_p are the electron and hole mobilities. The total electron and hole current density are the sum of drift and diffusion current density respectively which are described by Eq. 1-2 respectively. Eq. 1-3 shows the total current density. G represents the rates of generated

electron hole pairs by light exiting. R_n and R_p are the electron hole recombination rates. The continuity equations are determined by Eq. 1-4 and Eq. 1-5. The Atlas numerically solve these equations, and then derivate the I-V characteristics of solar cell.

1.4 Motivation

The solar spectrum consists of energies of wide range wavelengths. For efficient use of solar energy, multi-junction solar cells, such as double-junction (tandem) or triple-junction cells are used. The tandem solar cell can be fabricated with only silicon active layers and therefore makes it a preferable solar cell techniques. A tandem solar cell consists of a top and a bottom cell. A high bandgap material (a-Si:H) is used for the top cell, less thermalization losses occur as a result of absorption of high energy photons. The longer wavelength photons, which are not absorbed in the top cell, get absorbed in the bottom cell which consists of a lower bandgap material (μc-Si:H). Based on the review from the literature, we set up optical and electrical simulations for single-junction and tandem solar cell in order to compare with the realistic device and analyze the details of physics. Improvements regarding optical and electrical properties of the tandem solar cell are investigated to promote the performance of the solar cell.

From the experimental aspects, intrinsic hydrogenated microcrystalline silicon (μc-Si:H) has been shown to be a very promising new photovoltaic material for thin-film solar cells. However, the composition of μc-Si:H is complicated that it is hard to control the crystallinity. In this study we also try to control the crystallinity of μc-Si:H by modulating the growth parameters of PECVD to reach the crystallinity of 50% which is believed to be the optimized value reported by literatures.

Chapter 2

Literature Review

2.1 Silicon Thin Film Solar Cell

Several thin-film technologies have utilized silicon for the active material. Sticking to silicon instead of other semiconductors represents a number of advantages. Silicon is nontoxic, which makes it easily accepted by the public. Moreover, silicon is abundantly available in the earth crust, so that its availability (at least in its raw form) will never be an issue. Finally, silicon solar cell technologies can build further upon the extensive know-how accumulated over the years in the IC industry (for crystalline silicon) and the display industry (for amorphous and microcrystalline silicon). The term "thin-film silicon" is in fact quite broad. It covers a wide range of technologies from amorphous to microcrystalline silicon with thickness ranged from 0.1 to 5 μm. This section intends to give an overview of the solar cell technology containing amorphous and microcrystalline silicon thin film.

2.1.1 Single-Junction Amorphous Silicon Solar Cells

Amorphous silicon is usually deposited using the plasma-enhanced chemical vapour deposition (PECVD) technique, and the gas silane (SiH_4) is mostly used as precursor. As a result of decomposition, surface adsorption and surface reactions, a network of Silicon atoms is formed on the substrate, mostly glass or a metal foil. The deposition temperature ranges typically between 180°C and 280°C. As a result of the deposition mechanism, amorphous silicon contains a large concentration of hydrogen atoms (~10%). Hydrogen is, in fact, crucial for the material's electronic properties, while unhydrogenated amorphous silicon is of no use for devices. Therefore, the material one usually refers to using the words "amorphous silicon" is in fact hydrogenated amorphous silicon (a-Si:H). Amorphous silicon is a material that features short-range order but lacks long-range order. As in crystalline silicon, each silicon

atom is mostly fourfold coordinated, but the bond lengths and angles between the bonds show a wide variation. This structure has a strong impact on the electronic structure of the material. Because the structure is no longer periodic, the strict conservation of momentum does not hold. As a result, instead of the indirect bandgap of crystalline Si, it basically has a direct bandgap. Therefore the absorption coefficient in a-Si:H (1.7 to 1.9 eV) is much higher than that in crystalline Silicon. However, a-Si:H suffer from degradation upon exposure to sunlight [5]. This phenomenon, called the Staebler-Wronski effect, causes a large increase in defect density (strong decrease in excess carrier lifetime), and is reversible upon annealing at temperatures above 150 ^{o}C. From values between 10^{15} and 10^{16} cm^{-3} in annealed state, defect densities increase to ~2 x 10^{17} cm^{-3} in light-soaked state. The metastable defects are believed to be dangling bonds formed by breaking weak bonds in the random network. The defect densities mentioned are valid for intrinsic amorphous Silicon. Doped amorphous Silicon, obtained by adding diborane to the gas flow for p-type material and phosphine for n-type, contains much more defect than intrinsic a-Si:H (several orders of magnitude higher). Therefore, only intrinsic a-Si:H can be used as an absorber material. **Fig. 2-1** shows schematically the results obtained by W. E. Spear et al. [6] by plotting the values of dark conductivity and dark conductivity activation energy E_σ against gas phase doping ratio. Also plotted is the estimated position of the resulting Fermi level E_F, obtained by taking the E_σ values and correcting for the so-called statistical shift. The key parameters for amorphous Silicon are its dark conductivity, photoconductivity, and its mobility lifetime product. The conductivity of intrinsic a-Si:H in the dark is extremely low (< 10^{-10} S/cm) because of the low mobility (a-Si:H layer is around 20 cm^2/Vs at best), the large bandgap, and the fact that charge carriers at low concentration are trapped at defects. Under illumination, many of the defects get filled with photogenerated carriers and are saturated. As a result, many more charge carriers are available for charge transport, and the conductivity is many orders of magnitude higher than that in the dark. The photoersponse, defined as the ratio of the illuminated

conductivity to the dark conductivity, is a good indication for the suitability of the material for devices, and should be larger than 10^5.

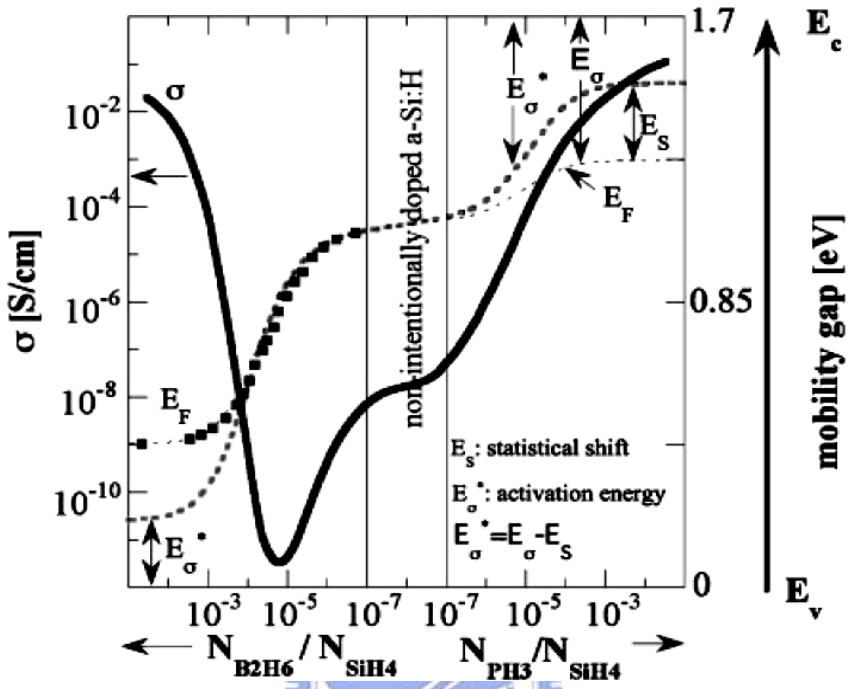

Fig. 2-1 The dark conductivity σ, activation energy E_σ, and estimated position of Fermi level E_F for a-Si:H, as a function of gas phase doping ratio N_{PH3}/N_{SiH4} (for n-type layers) and N_{B2H6}/N_{SiH4} (for p-type layers). E_σ* is the estimated 'true' distance between band edge (E_c, E_v) and the Fermi level E_F, where the statistical shift E_s has also been taken into consideration for n-type layers, assuming a constant defect density of 10^{16} /cm^2 eV. For p-type layers, an identical correction E_s has been assumed. In the graph, the equivalent bandgap of a-Si:H, or the 'mobility gap', is taken to be 1.7 eV.

The mobility lifetime (μτ) product is the crucial parameter for the transport properties of excess charge carriers in the layer, and in device grade, amorphous Silicon is larger than 10^{-7} cm^2/V. As a result of the low carrier mobility and low lifetime, collection cannot take place through diffusion. A strong drift field is an absolute requirement. Overall, it is not advisable to use amorphous silicon p–n-type diodes as solar cell structure for three reasons. (1) The doping

capability of a-Si:H is rather poor, the Fermi-level can be pushed only half way towards the conduction and valence band edges, even with heavy doping—this can be seen in **Fig. 2-1**. (2) Doping has a detrimental effect on a-Si:H layer quality, because it leads to the creation of many additional silicon dangling bonds, which are the main recombination centers in this material. (3) In a classical p–n-type solar cell, carrier collection is obtained by minority carrier diffusion within the p- and n-layers. Diffusion lengths in crystalline silicon wafers are sufficiently high (over 200 μm), to ensure carrier collection over the whole useful range of the solar cell thickness where significant optical absorption takes place. In a-Si:H layers, minority carrier diffusion lengths are extremely small (around 0.1 μm), and it becomes impossible for collection of photogenerated carriers on diffusion. Because of these three reasons, p–i–n diodes are always used for a-Si:H solar cells.

When modeling thin-film silicon devices, it is important to take into account the electronic structures of a-Si:H and μc-Si:H. The spatial disorder in the atomic structure of a-Si:H results in a continuous density of states (DOS) in the band gap with no well-defined conduction-band (CB) and valence-band (VB) edges. When considering the transport properties of charge carriers in a-Si:H, we have to distinguish between the extended states and the localized states in the DOS distribution as sketched in **Fig. 2-2**. The localized states within the mobility gap strongly influence the trapping and recombination processes; therefore, the trapped charge in the localized states cannot be ignored, as is often the case in the modeling of crystalline semiconductor devices. The localized states in the mobility gap of a-Si:H are represented by the CB and VB tail states and the defect states. These states are different in nature. The tail states behave like acceptor-like states (CB-tail states) or donor-like states (VB-tail states), and their density is described by an exponential decay into the mobility gap. The most common defect in a-Si:H is a dangling bond. A dangling bond can be in three charge states: positive (D^+); neutral (D^0); and negative (D^-). An imperfection with three possible charge states acts to a good approximation like a pair of two imperfections consisting

of a donor-like state ($DB^{+/0}$) and an acceptor-like state ($DB^{0/-}$), and is therefore represented by two so-called transition-energy levels $E^{+/0}$ and $E^{0/-}$ in the band gap. The continuous density of defect states is represented by two equal (Gaussian) distributions located around the middle gap. The corresponding pair of defect energy states is separated by the correlation energy. The different nature of the localized states in a-Si:H requires different approaches for the calculation of recombination-generation (R-G) statistics through these states. The models that are commonly used to describe the localized states in a-Si:H. The energy states in the bandgap act as trapping and recombination centers and therefore strongly affect many electronic properties of a-Si:H and the performance of a-Si:H devices. In contrast to crystalline semiconductors, in which the recombination process is typically dominated by a single energy level in the bandgap, in a-Si:H, contributions from all bandgap states to the recombination–generation (R–G) rate are included. In order to model the recombination process through the single level states, such as localized tail states, Shockley-Read-Hall R–G statistics is applied for the amphoteric defect states.

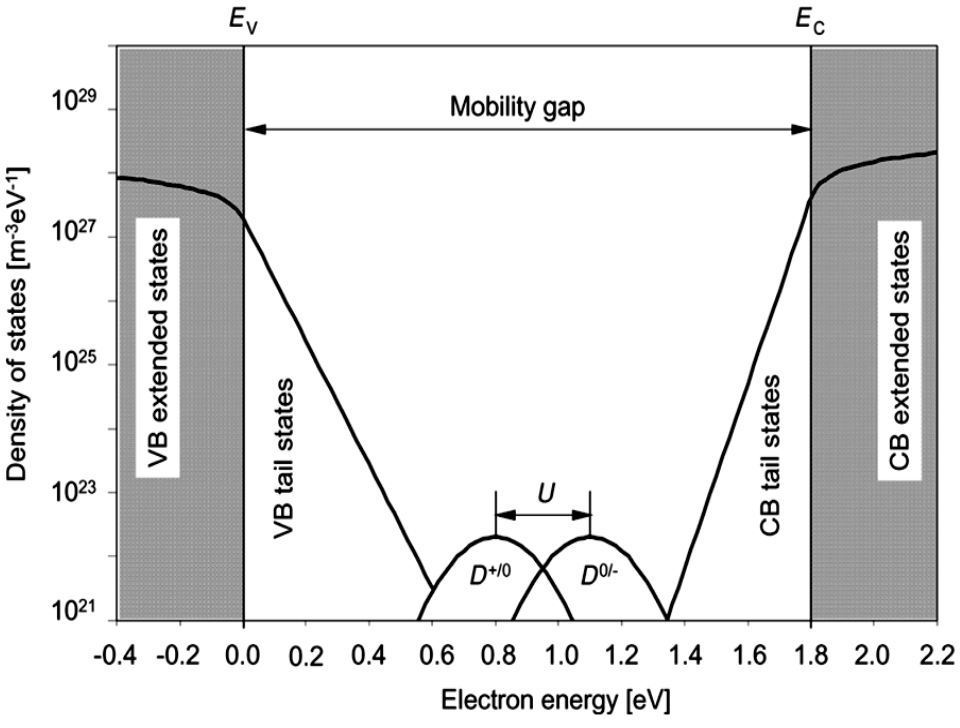

Fig. 2-2 Density of states of a-Si:H [4].

2.1.2 Single-Junction Microcrystalline Silicon Solar Cells

Microcrystalline is a mixed phase material, containing a crystalline silicon fraction and an amorphous silicon fraction. The crystallites are generally only a few nanometers to a few tens of nanometers in diameters, and are present in "bunches" or "conglomerates" in the layers. These conglomerates are much larger than the crystallites themselves, up to a micron or even larger. Because the crystallites are in the nanometer range, microcrystalline silicon is often referred to as "nanocrystalline silicon". The two names are nowadays used interchangeably. Like amorphous silicon, microcrystalline silicon contains a lot of hydrogen (several percents), which is incorporated in situ during deposition and ensures passivation of most defects in the layers. The term "microcrystalline silicon" covers, in fact, a whole range of materials, ranging from amorphous silicon with a few percents of crystalline phase to a material with only a few percents of amorphous silicon. The properties of the materials at the two extremes are quite different, and one has to pay attention not to generalize properties that are, in fact, only valid for a limited range of crystallinity. In practice, the best devices are obtained with material close to the edge between microcrystalline and amorphous Silicon, so most recent papers refer to this type of material, which contains a large amorphous fraction. Like amorphous Si, microcrystalline Silicon is typically obtained by PECVD at low temperature (between 100 and 300°C). Usually, a large hydrogen flow is added, which results in microcrystalline Si instead of amorphous Si ("hydrogen dilution"). The very high frequency (between 30 and 300 MHz) leads to a softer ion bombardment, which is more favorable to microcrystalline Si formation, and, at the same time, allows relatively high growth rates. It is, however, possible to obtain excellent results using the standard RF PECVD technique at 13.56 MHz, provided the right parameters in terms of pressure and gas flow are selected. The conditions used are the so-called "high pressure depletion" (HPD) conditions, where the relatively high pressure (~10 Torr) ensures that ions lose a lot of their energy before reaching the surface. It is important to ensure a high hydrogen content in the plasma in HPD

regime, which is usually obtained by a high hydrogen flow. The combination of Very High Frequency and HPD conditions has led to excellent solar cells. An important aspect for all deposition techniques is the need to control the crystallinity profile of the microcrystalline layer throughout the active layer. As the material is formed through nucleation from an initial amorphous silicon layer after which the crystallites grow, the crystallinity is not constant throughout the layer if no attempt is made to control it, which may result in far from optimal layers. Therefore, research in microcrystalline Silicon deposition puts a lot of effort into crystallinity control during deposition through varying Si the deposition parameters. The bandgap of microcrystalline silicon depends on the fraction of amorphous silicon in the material. Layers with a substantial crystalline fraction have a bandgap close to that of crystalline Silicon (1.1 eV). The apparent higher absorption for such microcrystalline layers compared to single crystalline Si has been demonstrated to be caused by light scattering at the layer surfaces. The absorption below the bandgap is much higher than that for crystalline silicon, and is caused by defects within the bandgap. The absorption coefficient at those long wavelengths, therefore, gives a measure for the layer quality. It can be measured in different ways, but a powerful measurement technique that is increasingly be being used is the Fourier transform photocurrent spectroscopy (FTPS) [7]. **Fig. 2-3** also gives important insight in layer quality degradation in microcrystalline silicon. When the first microcrystalline silicon solar cells were demonstrated, tests on devices with relatively high crystallinity led to the conclusion that microcrystalline Silicon did not suffer from light-induced degradation. As better devices closer to the transition were made and more detailed degradation studies were carried out, a more subtle picture has emerged: microcrystalline silicon suffers from a mild form of the photo-induced degradation [8]. The degraded values (after 1000 hours under standard illumination) in **Fig. 2-3** show that, as expected, the degradation is worst for fully amorphous silicon, while it is negligible for almost fully crystalline layers. For microcrystalline layers in the transition region, there is a small yet significant degradation.

There is, however, no degradation at all if the high energy photons are filtered out [9], as is the case in tandem solar cells. μc-Si:H with a higher crystalline volume fraction than a-Si:H. The assumption here is that the lower mobility band gap in μc-Si:H thin film cause the lower open circuit voltage. We would expect the free carrier densities to be higher in the bands for the "low Eg" μc-Si:H in which the band edges are closer to the quasi-Fermi levels. This is easily inferred from the expressions of the free carrier densities:

$$n = N_C e^{-(E_C - E_{Fn})/KT} \quad \text{Eq. 2-1}$$

$$p = N_V e^{-(E_{Fp} - E_V)/KT} \quad \text{Eq. 2-2}$$

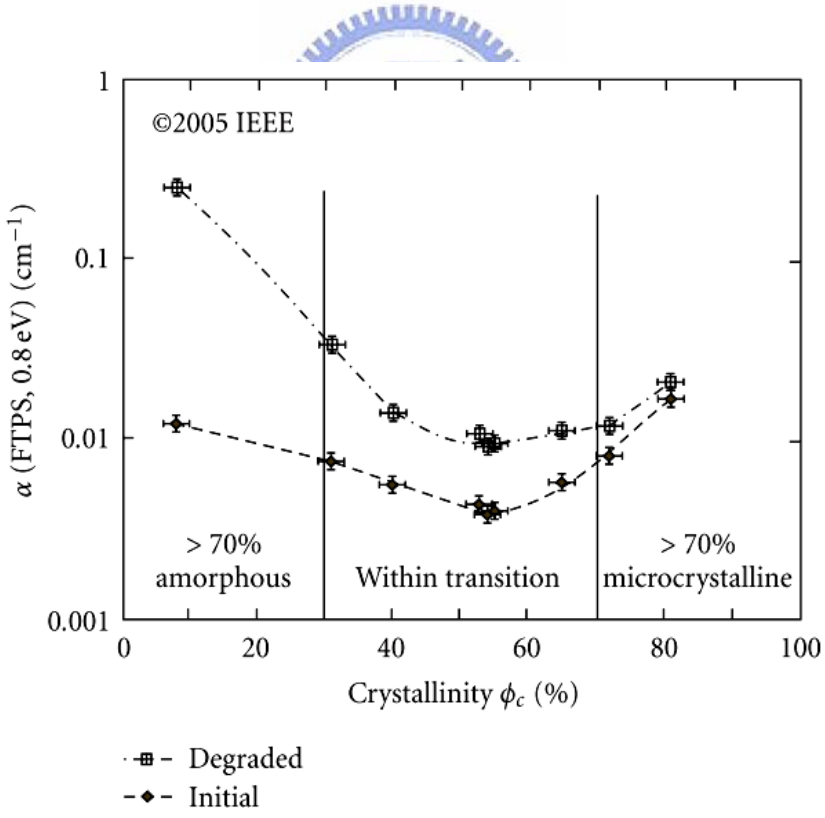

Fig. 2-3 Defect-related optical absorption in as-deposited and degraded state for a series of single-junction μc-Si:H silicon p-i-n solar cells as a function of the crystallinity of the intrinsic layer (i-layer) [8].

In the general, a μc-Si:H cell with a higher crystallinity has a higher Jsc, primarily because of higher free carrier mobilities and higher free carrier densities, which causes higher photo-generated hole trapping, therefore higher field near the P/I interface, and a collapse of the electric field over the volume and a lower V_{oc}. In fact the above opinions are the reasons for a lower V_{oc} and higher J_{sc} in μc-Si:H cells [11].

2.1.3 Tandem Solar Cell

Microcrystalline silicon has not only the advantage of a better stability under light exposure than amorphous silicon. Microcrystalline silicon has a different sunlight absorption spectrum than a-Si:H as shown in **Fig. 2-4**.

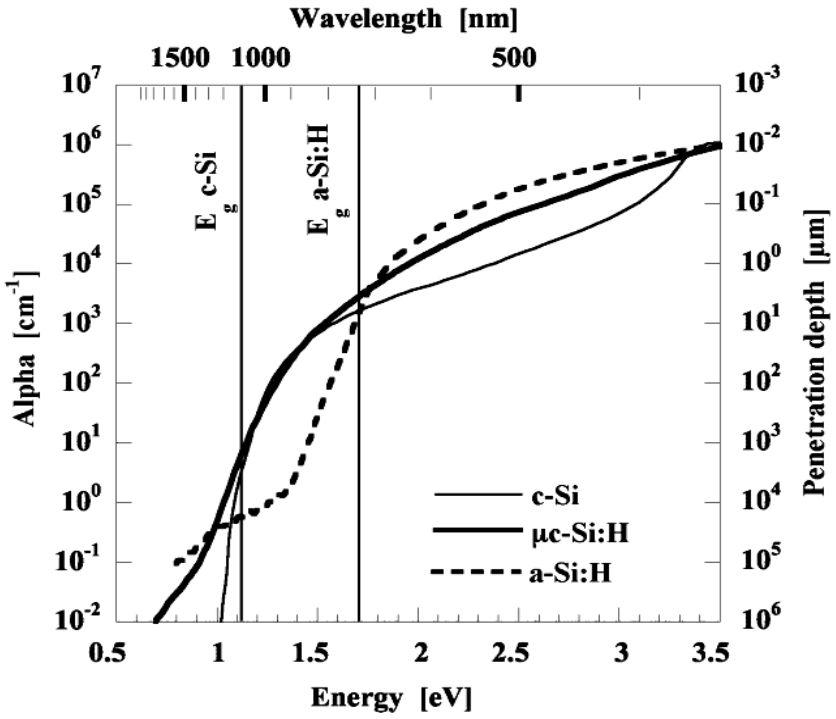

Fig. 2-4 The optical absorption coefficient α and the penetration depth d_λ, where $d_\lambda = 1/\alpha$ of monochromatic light with photon energy hυ and wavelength λ, for crystalline silicon (c-Si), and typical device-quality a-Si:H and μc-Si:H layers on glass. The curve for μc-Si:H has been corrected for light scattering due to surface roughness [10].

μc-Si:H absorbs the light more in the infrared range. This difference between a-Si:H and μc-Si:H has been used to increase the sunlight energy conversion efficiency by performing a so-called Tandem cell, which consists in a multi-junction cell with a top-cell made of a-Si:H and a bottom-cell of μc-Si:H. The thickness of the a-Si:H intrinsic layer is generally thin (about 250 nm) in order to collect a maximum of the photo-induced electrons. The μc-Si:H intrinsic layer has to be thicker (about 1.5 - 2 μm) because of its indirect band-gap and the necessity to match the photo-current generated by the two stacked cells [2].

From the point of view of the manufacturing technique, μc-Si:H is fully compatible with a-Si:H. Indeed, it can be deposited using the same reactor at the same substrate temperature of about 200 °C. The source gases are silane and hydrogen as for the deposition of a-Si:H. Generally, the hydrogen dilution is increased to change from the amorphous to the microcrystalline silicon deposition regime. When μc-Si:H is deposited in RF PECVD, the deposition rate (1 - 5 Å/s range) is generally less than for a-Si:H. This low deposition rate is a limiting factor for the use of μc-Si:H in PV solar cells, because it involves a too long time to deposit the ~ 2 μm thick μc-Si:H intrinsic layer. Typically, about 1.5 hours are necessary to deposit a 2 μm thick layer with a 4 Å/s deposition rate. In order to achieve low-cost Tandem PV solar cells, the deposition rate of the intrinsic μc-Si:H layer has to be improved to rates higher than 10 Å/s. High deposition rates are not the only condition for μc-Si:H films to achieve low-cost Tandem PV solar cells. Vetterl et al [12] have shown that the best material quality to be integrated in a Tandem solar cell is at the limit between amorphous and microcrystalline silicon. Therefore, the deposition conditions have to be perfectly controlled in order to have a material crystallinity in the 40 - 60 % range, and not to fall into the fully amorphous or strongly microcrystalline deposition region.

2.2 Deposition Mechanisms of μc-Si:H Thin Film

The mechanisms involved in the growth of hydrogenated microcrystalline silicon are complex, which combine both chemical and physical aspects. The chemical aspects include the hydrogen, silicon dangling bonds and reactions in the film. The physical aspects is such as the species (SiH_x and H) bulk diffusion. The heterogeneous microstructure composed by crystalline grains embedded in an amorphous matrix adds to the system complexity. Moreover, the surface and sub-surface chemistry and physics depend on both the growing film properties and on the plasma. The three most important models are *the surface diffusion model*, t*he selective etching model* and *the chemical annealing model*, which are reviewed in this section.

2.2.1 Surface Diffusion Model

The surface diffusion model was experimentally demonstrated as shown by Matsuda [46]. The crystalline volume fraction of deposited films strongly depends on the surface diffusivity of SiH_x which is improved when the silane concentration is reduced or the substrate temperature increased. This is due to the hydrogen surface coverage improvement prolong the SiH_x surface diffusion length to permit SiH_x to attach at favorable sites to create a flat film surface. This has been confirmed by the abrupt fall of the film crystallinity for substrate temperature higher than 400 ◦C [13], caused by the desorption of hydrogen adsorbed on the surface at such high temperatures [14]. Moreover, some of the hydrogen atoms coming from the plasma recombine with surface bonded-hydrogen heating locally the surface, which enhances the surface diffusion of SiH_x as sketched in **Fig. 2-5**. The role of the surface diffusion in flattening the film surface is of particular importance for the nucleation of crystallites as shown by in-situ spectroscopic ellipsometry studies.

They have shown that silicon crystallite nucleation needs a smooth surface and occurs only after a reduction of the initial surface roughness. This shows that to promote the

crystallinity of the deposited silicon film, a sufficiently high atomic hydrogen flux towards the growing film surface has to be delivered with respect to the silicon radicals flux. However, the role of the SiH_x surface diffusion in μc-Si:H growth may not be dominant for depositions performed at high rates, because of the shorter time allowed for SiH_x radicals to find adequate sites to attach.

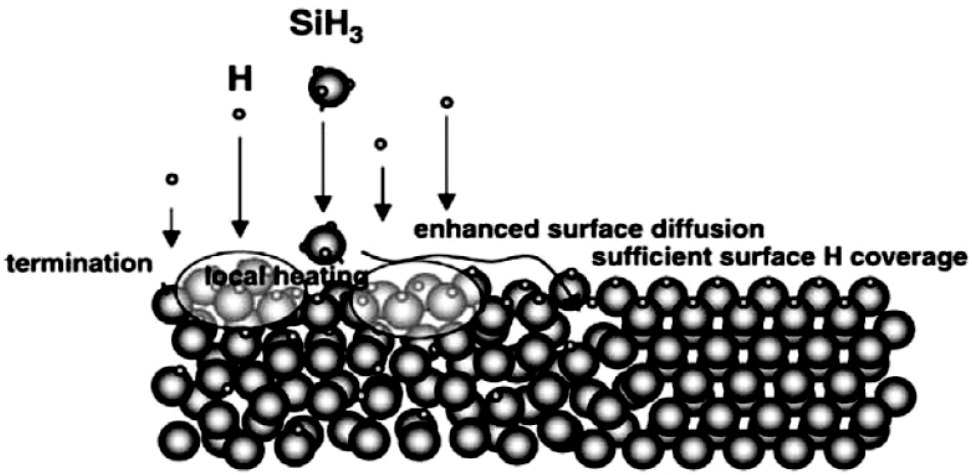

Fig. 2-5 Schematic representation of the surface diffusion model. The hydrogen atoms from the plasma passivate all the surface dangling bonds, hence enhancing the surface diffusion length of silicon radicals, which have to find an adequate site to attach [15].

2.2.2 Selective Etching Model

The diffusion model was able to explain μc-Si:H deposition for substrate temperatures lower than 400◦C, but μc-Si:H deposition at higher temperatures [16] shows that this model is not sufficient. A combination of the surface diffusion model and selective etching model may explain the deposition of microcrystalline silicon. This selective etching model is based on the experimental observation of silicon etching by hydrogen [17] by the reverse chemical reaction leading to silicon deposition from silane discharge [18].

$$SiH_4 \underset{\text{etching}}{\overset{\text{deposition}}{\rightleftharpoons}} Si_{\text{film}} + 4\,H \qquad \text{Eq. 2-3}$$

This model is called selective because of the different etching rate of amorphous and microcrystalline silicon [17]. Indeed, the high lattice defect density in the amorphous structure facilitates the atomic hydrogen to etch the silicon atoms which are weakly bonded to their neighbors, whereas the well-arranged silicon atoms of the crystallites resist better to hydrogen etching [15]. The selective etching model sketched in **Fig. 2-6** is based on the hypothesis that both amorphous and microcrystalline silicon are deposited and etched simultaneously, but with an etching rate much higher for the amorphous phase, hence increasing the crystalline volume fraction of the growing film. This model has to be combined with the surface diffusion model in order to explain the nucleation of the crystallites to initiate the microcrystalline growth from the initial amorphous incubation layer. As for the surface diffusion model, the crucial physical consideration is the atomic hydrogen flux towards the film surface with regard to the silicon radical flux, in order to etch efficiently the amorphous phase to promote the film crystallinity.

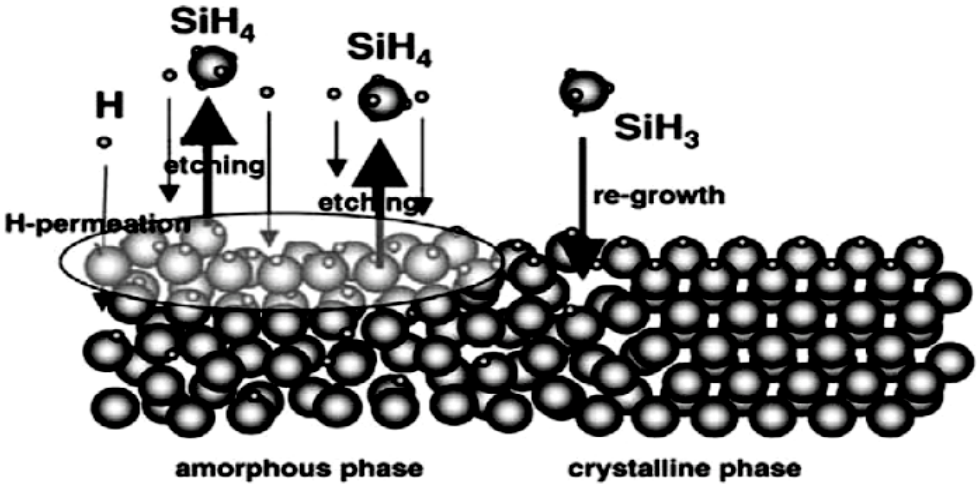

Fig. 2-6 Schematic representation of the selective etching model. The hydrogen atoms from the plasma etch preferentially the amorphous silicon phase, favoring the growth of the crystalline phase, resulting in μc-Si:H [15].

2.2.3 Chemical Annealing Model

The chemical annealing model has been constructed in order to explain the crystallization of amorphous silicon when exposed to a pure H_2 plasma [19]. Indeed, μc-Si:H can be produced by using a layer-by-layer technique by alternatively depositing a thin a-Si:H layer and expose it to a pure H_2 discharge which crystallizes the thin layer. Neither the etching model, nor the surface diffusion model, can explain this phenomenon. This third model is based on the chemical reaction of atomic hydrogen coming from the plasma with hydrogen bonded to silicon at the film surface or sub-surface as depicted in **Fig. 2-7**. The reaction creates a silicon dangling bond and a hydrogen molecule. This reaction is exothermic, and the resulting structure thermal vibration promotes surface and bulk structural rearrangement leading to the energetically more favorable μc-Si:H [15]. The Si dangling bond created is then transformed into a more stable and rigid Si-Si bond or, if placed at thefilm surface, re-hydrogenated by atomic hydrogen from the plasma. In the selective etching model, the H atoms attach to silicon and re-hydrogenate the bulk silicon until silane desorption. But in the chemical annealing model, the H atoms recombine with surface or sub-surface hydrogen.

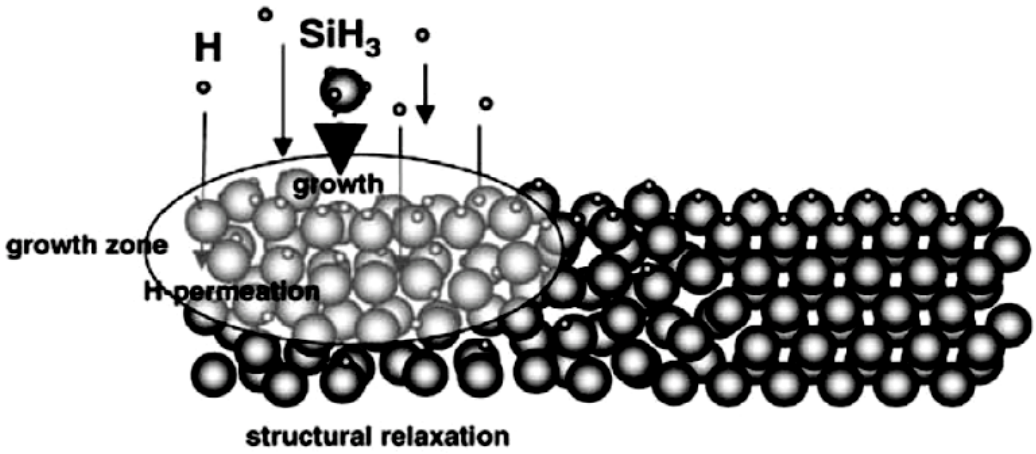

Fig. 2-7 Schematic representation of the chemical annealing model. The hydrogen atoms from the plasma recombine with hydrogen bonded to surface or sub-surface silicon atoms, delivering vibrational energy which favors silicon crystallization [15].

Consequently, the atomic hydrogen flow rate towards the surface has to be large compared to the silicon radical flux to promote the growth of μc-Si:H. This is to increase the surface diffusivity by a fully H-covered surface, to remove undesirable a-Si:H by selective etching by H atoms, or to generate vibrational energy by hydrogen surface or sub-surface recombination, according to the surface diffusion, the selective etching or the chemical annealing models, respectively.

Chapter 3

Experimental Technique

3.1 Plasma-Enhanced Chemical Vapor Deposition

The deposition method used to produce the μc-Si:H film is rf (the excitation frequency is 27.12MHz)PECVD. The plasma provides some of the activation energy required for the chemical reaction, in effect reducing the processing temperature required during the film deposition. It is done by collisions with electrons, which originate as secondary electrons in the plasma and build up their energy by acceleration in an electric field. The μc-Si:H film is deposited by attaching reactive particles of dissociated silane molecules, called radicals, to the surface of growing film. Some of the energy transferred to silane molecules in the collisions with electrons is radiated as visible light, for which reason the deposition method is also referred to as glow discharge.

3.2 Raman Spectrum

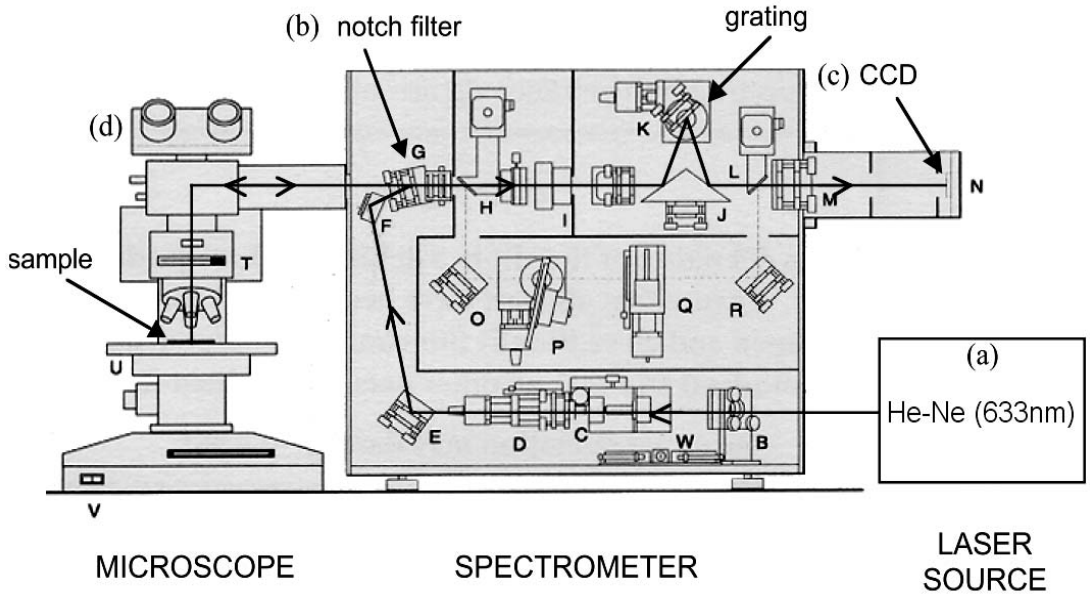

Fig. 3-1 Micro-Raman spectrometer composed of an He-Ne laser source, a microscope, a notch filter, a grating and a CCD camera [20].

Raman spectroscopy consists in the observation of inelastic scattering of an incident light beam by a media which could be a gas, a liquid or a solid. The Raman effect, first reported by Raman and Krishna in 1928 [20], has been used in this work to evaluate the degree of crystallinity of the deposited silicon layers. The Raman apparatus was a Renishaw RM series with an He-Ne laser source (633 nm).

Silicon films with mixed amorphous-nanocrystalline phase composition, the spectrum consists of a broad low-frequency component peaking around 480 cm^{-1} and related to the amorphous phase and a substantially narrower peak at 520cm^{-1} whose increase in intensity indicates nucleation of the nanocrystalline phase. The total scattering intensity $I(\omega)$ in the frequency range under study can be written as the formula.

$$I(\omega) = I_c(\omega) + I_a(\omega) \qquad \text{Eq. 3-1}$$

where $I_c(\omega)$ is the intensity of the line related to the nanocrystalline phase (520cm^{-1}), and $I_a(\omega)$ is that of the line associated with the amorphous phase (480 cm^{-1}).

Now, considering the relation between the integrated raman intensity and the volume fractions of the amorphous and nanocrystalline phases. This relation is usually written in the **Eq. 3-2**, where y is the scattering factor.

$$X_c = \frac{I_c / I_a}{y + I_c / I_a} \qquad \text{Eq. 3-2}$$

An empirical relation for the dependence on Eq. 3.4, We used the value $y = 1$ [21].

$$L : y(L) = 0.1 + \exp(-L/25) \qquad \text{Eq. 3-4}$$

And this is a good agreement with the estimate y=0.88. Thus the formula of crystallinity is described as Eq. 3.5.

$$X_c = \frac{I_c}{I_c + I_a} \quad . \qquad \text{Eq. 3-5}$$

Chapter 4

Results and Discussions

4.1 Hydrogenated Amorphous Si Solar Cell

Hydrogenated amorphous Si (a-Si:H) material have received a great attention because of their use in low-cost solar cells. In order to analyze and optimize the performance of thin-film a-Si:H solar cells, it is important to set up an accurate numerical model to simulate the transport mechanisms in the device. Device simulation comprises methods of basic carrier transport and continuity equations for any type of structures defined by two dimensional doping profiles. Silvaco (Atlas), which is based on finite element analysis, is widely used by research institutes and industries. Through Atlas, we input several parameters including: device structure, doping concentration, and bias condition; then, using numerical methods such as: electron and hole current equation, electron and hole continuity equations, and Poisson equation; finally getting the outputs like mobile carriers, electric fields, potentials, and currents in the form of two-dimensional contours and vectors as well as quasi three-dimensional contours. Besides simulating the external current-voltage characteristics, it allows a detailed simulation of physical behaviors of devices in both steady-state and in transient regime. Device simulation has been widely used to study a-Si:H p-b-i-n solar cell performance, which is sensitive to the material properties.

4.1.1 Simulation Model

The physical models that we have used are Klaassen's concentration dependent SRH model (KLASRH), Klaassen's Auger model (KLAAUG), Klaassen's concentration dependent lifetime model, and Klaassen's low field mobility model (KLA). The photo-generation model which includes a ray tracing algorithm is used to calculate the transmission and absorption of light in the bulk as well as reflection and refraction at the interfaces. The p-i-n solar cell is

operated under the global standard solar spectrum (AM 1.5G) illumination with total incident power density which is 100 mW/cm^2 and the light intensity for each wavelength is calculated in the wavelength from 0.3 to 1.2 μm. A structure consists of flat glass/ITO/a-Si:H p-i-n/Ag, is considered as the solar cell model for simulation, in which light penetrate through the p-layer. The figure is shown as **Fig. 4-1**.

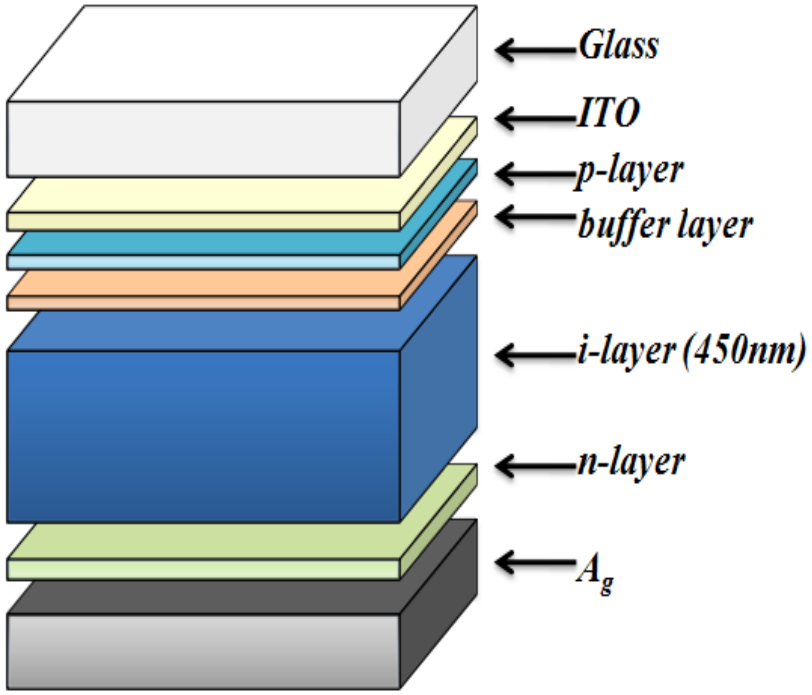

Fig. 4-1 Schematics of an a-Si solar cell structure, which consists of glass/ITO/a-Si:H p-i-n/Ag

We set the solar cell in length and width both as 1 μm . The thicknesses of i-layer is 450 nm. We assumed that interfaces are all flat for this simulation. The doping concentration of p- and n-type set as 3x10^{18} cm^{-3} and 9x10^{18} cm^{-3}at first. Each dangling bond density in p-layer and n-layer is set as 5x10^{18} cm^{-3} and 9x10^{18} which is higher than that in other layers. It is because the dangling bond density would increase with higher doping concentration in a-Si:H material. Also, we have analyzed the effect of light soaking would increase dangling bond density (N_{db}) in a-Si:H layer. The electrical, optical, and structural parameters in the

Table 4-1 which were adapted from the literature [22, 23] are used for simulating the device performance. The distribution of density of states (DOS) in the forbidden energy gap of undoped a-Si:H i-layer is used in the simulation.

Table 4-1 Device Parameters of a-Si:H solar cell used in Simulations.

Parameter	p-a-SiC:H	b-a-SiC:H	i-a-Si:H	n-a-Si:H
Layer thickness (nm)	5~20	1~10	250~500	10~30
Mobility gap (eV)	2	1.96	1.86	1.8
Donor doping density (cm^{-3})				$3x10^{18}$
acceptor doping density (cm^{-3})	$9x10^{18}$			
Electron mobility(cm^2/V s)	20	20	20	20
Hole mobility(cm^2/V s)	4	4	4	4
Electron life time (μs)	0.01	0.01	0.01	0.01
Hole life time (μs)	0.1	0.1	0.1	0.1
Effective DOS in the valance and conduction bands (cm^{-3})	$2x10^{20}$	$2x10^{20}$	$2x10^{20}$	$2x10^{20}$
Exponential tail Prefactors NTD, NTA ($cm^{-3}eV^{-1}$)	$4x10^{21}$	$4x10^{21}$	$4x10^{21}$	$4x10^{21}$
Characteristic energy WTD (VB tail) (eV)	0.12	0.11	0.08	0.05
Characteristic energy WTA (CB tail) (eV)	0.07	0.055	0.05	0.03
Gaussian distribution density NGD, NGA ($cm^{-3}eV^{-1}$)	$5x10^{18}$	$5x10^{17}$	$5x10^{15}$	$9x10^{18}$
Characteristic energy for Gaussian distribution WTD (donor like state) (eV)	0.2	0.2	0.2	0.2
Characteristic energy for Gaussian distribution WTA (acceptor like state) (eV)	0.2	0.2	0.2	0.2
Peak of donor like Gaussian distribution EGD (eV)	0.8	0.82	0.83	0.78
Peak of acceptor like Gaussian distribution EGA (eV)	0.9	0.67	0.67	0.52
Correlation energy U (eV)	0.3	0.47	0.36	0.5
Transmittance of glass / ITO	0.9			
Reflectivity of n layer / metal contact				0.9
Surface recombination velocity	$1x10^7$			$1x10^7$

[a] measured from the conduction band edge ; [b] measured from the valance band edge

Fig. 4-2 is the general standard model for DOS of a-Si:H i-layer and is described by :

1. A parabolic conduction band and exponentially decaying conduction band tail.

$$g_{TA}(E) = NTA \exp\left[\frac{E - E_C}{WTA}\right] \qquad \text{Eq. 4-1}$$

2. A parabolic conduction band and exponentially decaying conduction band tail.

$$g_{TD}(E) = NTD \exp\left[\frac{E_V - E}{WTD}\right] \qquad \text{Eq. 4-2}$$

3. Two equal Gaussian distributions of states around the middle gap separated from each other by a correlation energy (U) for representing the defect state related to dangling bonds ($DB^{+/0}$ and $DB^{0/-}$).

$$g_{GA}(E) = NGA\left[-\left[\frac{EGA - E}{WGA}\right]^2\right] \qquad \text{Eq. 4-3}$$

$$g_{GD}(E) = NGD\left[-\left[\frac{E - EGD}{WGD}\right]^2\right] \qquad \text{Eq. 4-4}$$

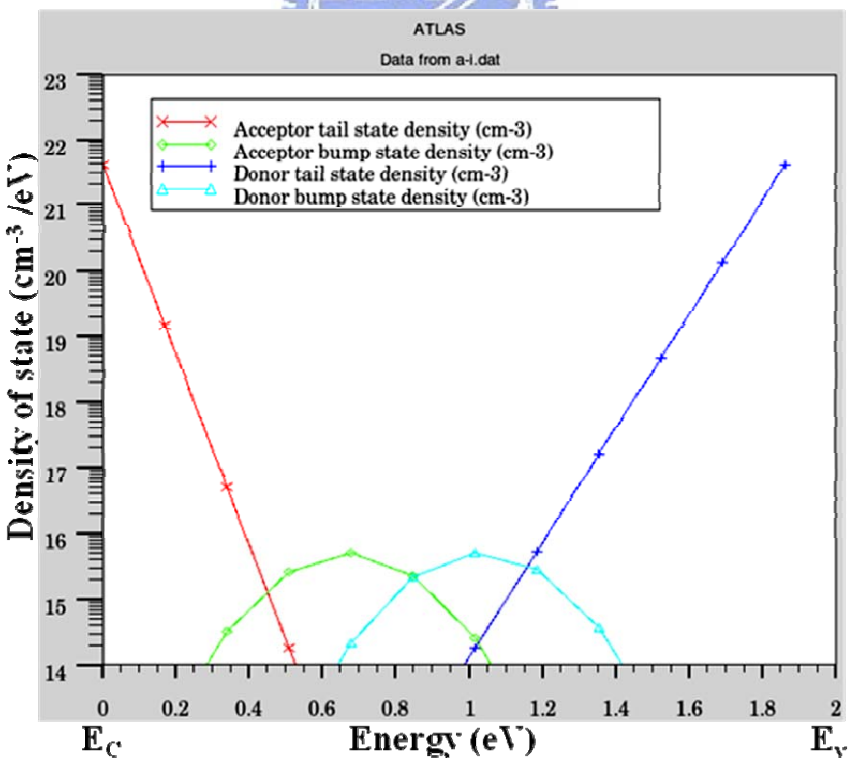

Fig. 4-2 Distribution of acceptor/donor-like trap states across the forbidden energy gap used in i-layer in the simulation.

The device performance of the a-Si:H solar cell is studied by using Atlas. The electric characteristics of a-Si:H solar cell are as following:

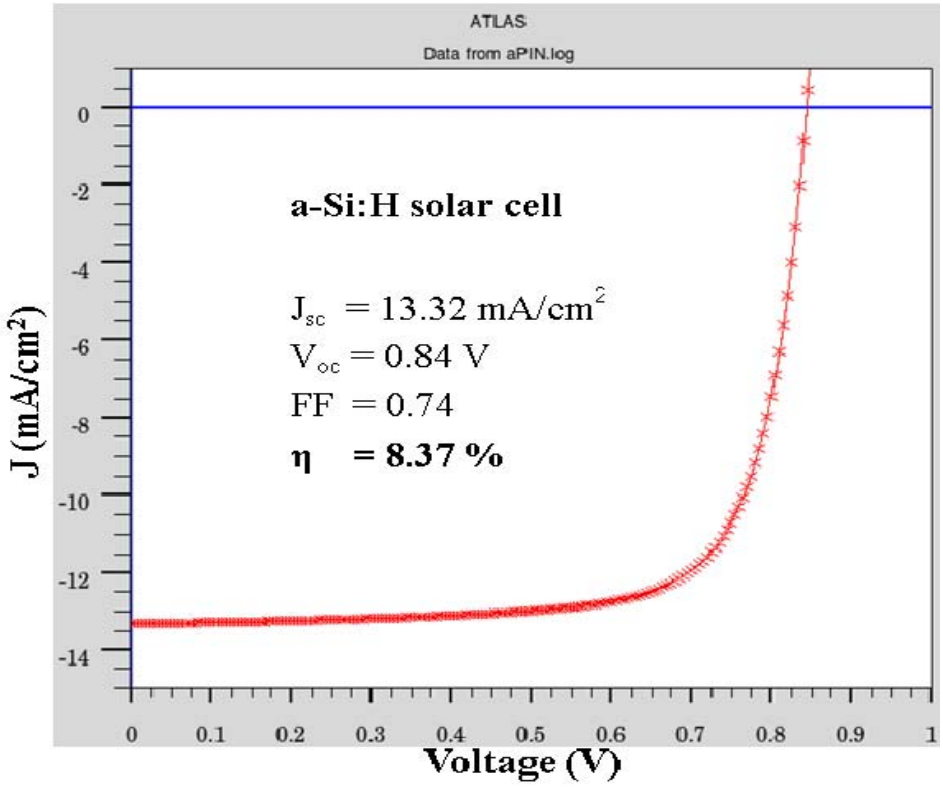

Fig. 4-3 The illuminated J-V characteristic curve of a-Si:H p-i-n solar cell

The computer simulation of a-Si:H p-i-n solar cell was carried out by atlas. The short circuit current (J_{sc}), open circuit voltage (V_{oc}), fill factor (FF), and the efficiency of a-Si:H solar cell are 13.3 mA/cm^{-2}, 0.83V, 0.74, and 8.37 %, respectively in **Fig. 4-3**. We considered the lower efficiency resulted from two reasons. First, the flat interfaces would reduce the light refraction and reflection. Second, the lack of TCO between the n-layer/Ag interface also made the efficiency low. The performance of the cell within light soaking effect is analyzed by increasing N_{db} from $5x10^{15}$ cm^{-3} to $5x10^{18}$ cm^{-3} as shown in **Fig. 4-4** and **Fig. 4-5**. The open-circuit voltage V_{oc}, fill factor FF, and short-circuit density J_{sc} were all decreased due to the N_{db} increased. a-Si:H would degrade upon exposure to sunlight. This phenomenon, called the Staebler-Wronski effect or light soaking effect, causes large increases in defect density and is reversible when annealed at temperatures above 150 ^{o}C. The metastable defects are

believed as dangling bonds formed by breaking weak bonds in the random network. In order to eliminate this effect, reducing i-layer thickness and hydrogen content in the film are two better ways so far. Thus, the a-Si:H i-layer of tandem solar cell is also designed to be thinner to achieve this purpose.

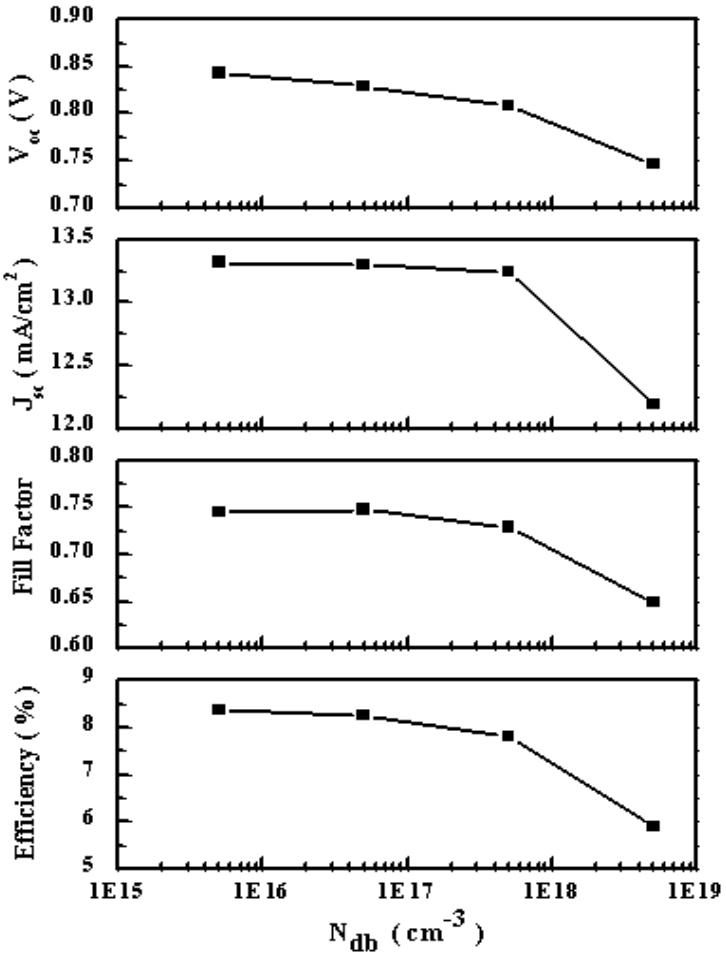

Fig. 4-4 Photovoltaic performance of a-Si:H solar cell with different N_{db} of i-layer.

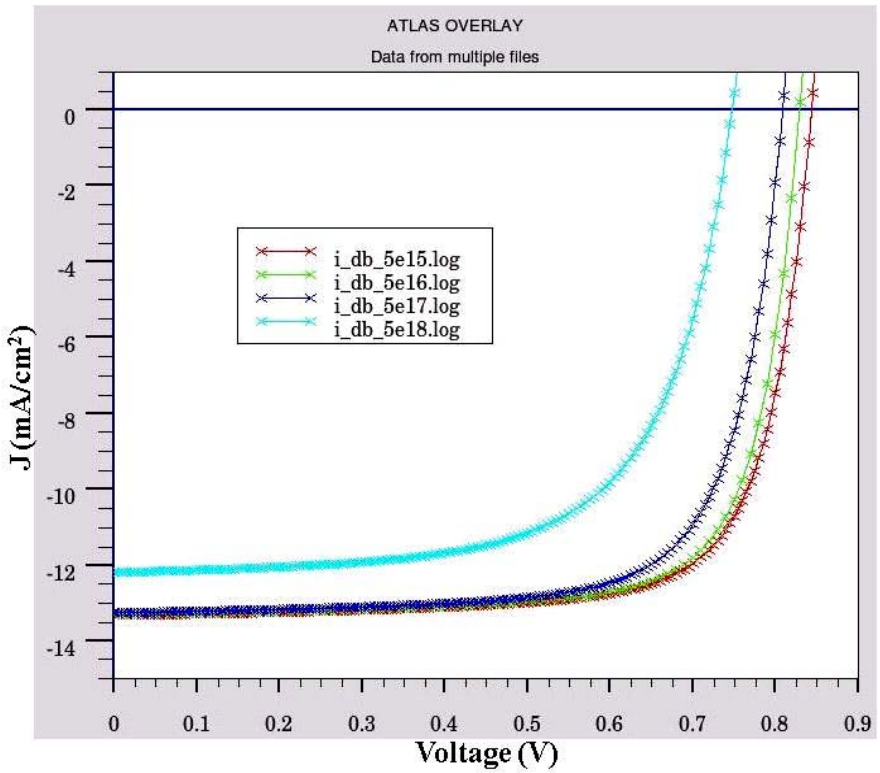

Fig. 4-5 The J-V characteristics curve with different N_{db} in i layer of a-Si:H cells.

4.2 Microcrystalline Silicon solar cell

The structure of microcrystalline p-i-n solar cell is as following: flat ITO/p-μc-Si:H / i-μc-Si:H/n-a-Si:H/Ag. The open-circuit voltage, short-circuit current density, and the fill factor determine the output properties of a solar cell; however, unlike the other two parameters, the behavior of the open-circuit voltage (V_{oc}) is not easy to be understood. It is well known the V_{oc} in hydrogenated microcrystalline silicon (μc-Si:H) thin-film solar cell declines sharply when the crystalline fraction increases from 60% to 90% or even higher. The tendency of different crystallinities of μc-Si:H cells has been studied until now, but it still lacks detailed quantification of the impact of individual material properties on solar cells. Here, we used a powerful electrical-optical computer modeling program (Atlas) to simulate the optimal μc-Si:H thin-film solar cells to understand the difference between the a-Si:H and μc-Si:H solar cell.

4.2.1 Simulation Model

The μc-Si:H solar cell structure is shown as **Fig. 4-6**. The length and width of solar cell are both set as 1 μm . The thicknesses of i-layer is 2200 nm. We assumed that interfaces are all flat in this simulation. Each doping concentration of p- and n-type initially set as $1x10^{19}$ $cm^{-3}$and $3x10^{18}$ $cm^{-3}$to optimize cell performance.

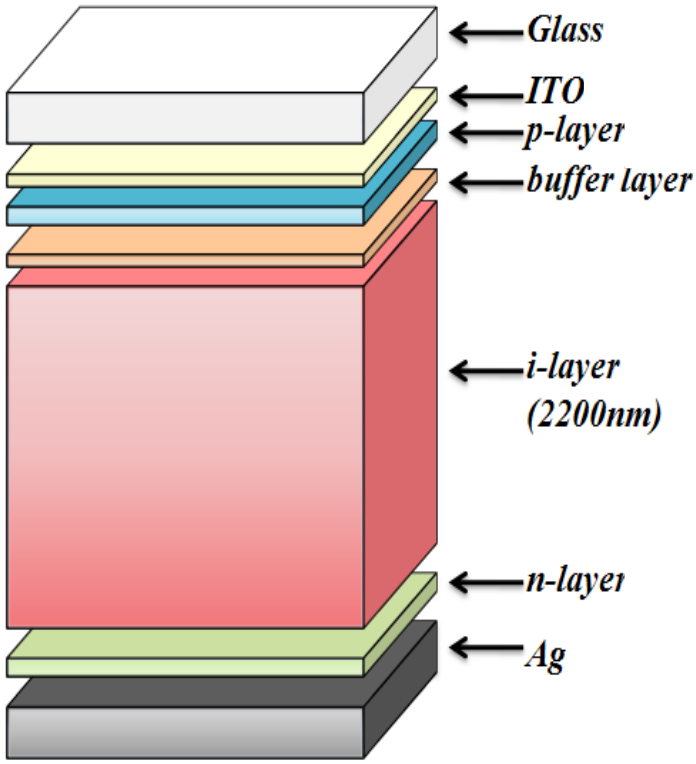

Fig. 4-6 μc-Si:H solar cell structure.

To model all aspects of the solar cell performance accurately, we had to assume that the more crystallized material has a lower band gap, higher carrier mobilities, and both higher mid-gap defect density and narrower band tails. A lower band gap for more crystallized μc-Si:H has been previously measured [24] by in situ Kelvin probe analysis and the "Flat Band Hetero-junction" technique; it also measured by photoluminescence (PL) in the study of Merdzhanova et al. [25] . In a-Si:H, the bonding length and bonding angle altered slightly but still in rule in short range, whereas atoms arrange randomly in long range. It makes the tail distribution is broader than the crystalline material. The physical simulation model are

Klaassen's concentration dependent SRH model (KLASRH), Klaassen's Auger model (KLAAUG), Klaassen's concentration dependent lifetime model, and Klaassen's low field mobility model (KLA).

Table 4-2 Device Parameters of μc-Si:H solar cell used in Simulations.

Parameter	p-μc-Si:H	b-μc-Si:H	i-μc-Si:H	n-a-Si:H
Layer thickness (nm)	10~30	5~10	1500~2500	10~20
Mobility gap (eV)	1.2	1.4	1.4	1.8
Donor doping density (cm-3)				$3x10^{18}$
acceptor doping density (cm-3)	$1x10^{19}$			
Electron mobility(cm2/Vs)	100	32	32	20
Hole mobility(cm2/Vs)	25	8	8	4
Electron life time (μs)	0.01	0.01	0.01	0.01
Hole life time (μs)	0.1	0.1	0.1	0.1
Effective DOS in the valance and conduction bands (cm^{-3})	$2x10^{20}$	$2x10^{20}$	$2x10^{20}$	$2x10^{20}$
Exponential tail Prefactors NTD, NTA ($cm^{-3}eV^{-1}$)	$4x10^{21}$	$4x10^{21}$	$4x10^{21}$	$4x10^{21}$
Characteristic energy WTD (VB tail) (eV)	0.04	0.045	0.05	0.05
Characteristic energy WTA (CB tail) (eV)	0.02	0.025	0.03	0.03
Gaussian distribution density NGD, NGA ($cm^{-3}eV^{-1}$)	$5x10^{18}$	$3x10^{17}$	$4x10^{16}$	$9x10^{18}$
Characteristic energy for Gaussian distribution WGD (donor like state) (eV)	0.2	0.2	0.2	0.2
Characteristic energy for Gaussian distribution WGA (acceptor like state) (eV)	0.2	0.2	0.2	0.2
Peak of donor like Gaussian distribution EGD (meas. From Valance edge) (eV)	0.4	0.7	0.7	1
Peak of acceptor like Gaussian distribution EGA(meas. From Conduc. edge) (eV)	0.6	0.5	0.5	0.6
Correlation energy U (eV)	0.2	0.2	0.2	0.2
Transmittance of glass / ITO	0.9			
Reflectivity of n layer / metal contact				0.9
Surface recombination velocity	$1x10^{7}$			$1x10^{7}$

[a] measured from the conduction band edge ; [b] measured from the valance band edge

The photogeneration model, which includes a ray tracing algorithm, is used to calculate the transmission and absorption of light in the bulk as well as reflection and refraction at the interfaces. The μc-Si:H solar cell is operated under the global standard solar spectrum (AM 1.5G) illumination with 100 mW/cm^2 total incident power density and the light intensity for each wavelength is calculated in the wavelength ranger from 0.3 to 1.2 μm. **Table 4-2** indicates electrical, optical and structural parameters used for simulating the device performance [26].

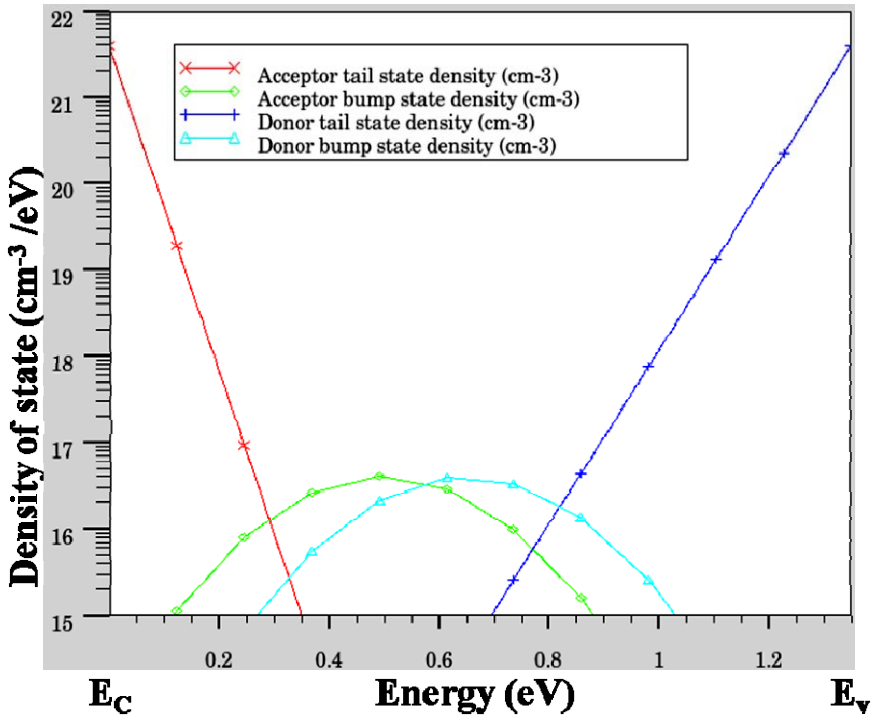

Fig. 4-7 Distribution of acceptor/donor-like trap states across the forbidden energy gap used in i-layer in the simulation study.

Fig. 4-7 is the general standard model for DOS of μc-Si:H i-layer. We assumed the Gaussian defect density in μc-Si:H i-layer is 4x10^{16} cm^{-3} which is higher than in a-Si:H i-layer (5x10^{15} cm^{-3}), because the defects fill with the grain boundaries. Due to the μc-Si:H material, it makes lower band gap, sharper band tails and higher Gaussian defect density. Simulation

results indicate a higher J_{sc} but lower V_{oc} in higher crystallinity material as shown in **Fig. 4-8**. The short current ,open voltage, fill factor, and the efficiency of a-Si:H solar cell are 21.81 mA/cm^2, 0.47V, 0.73, and 7.49 %, respectively. As we have stated, the electrical characteristics are differ from the a-Si:H solar cell in **Table 4-3**. The crucial point to reach solar grade quality µc-Si:H is to have good quality grain boundaries containing a low amount of unstable defects. Indeed, low quality amorphous silicon grain boundaries or cracks along grain boundaries which can be observed in highly-crystalline µc-Si:H.

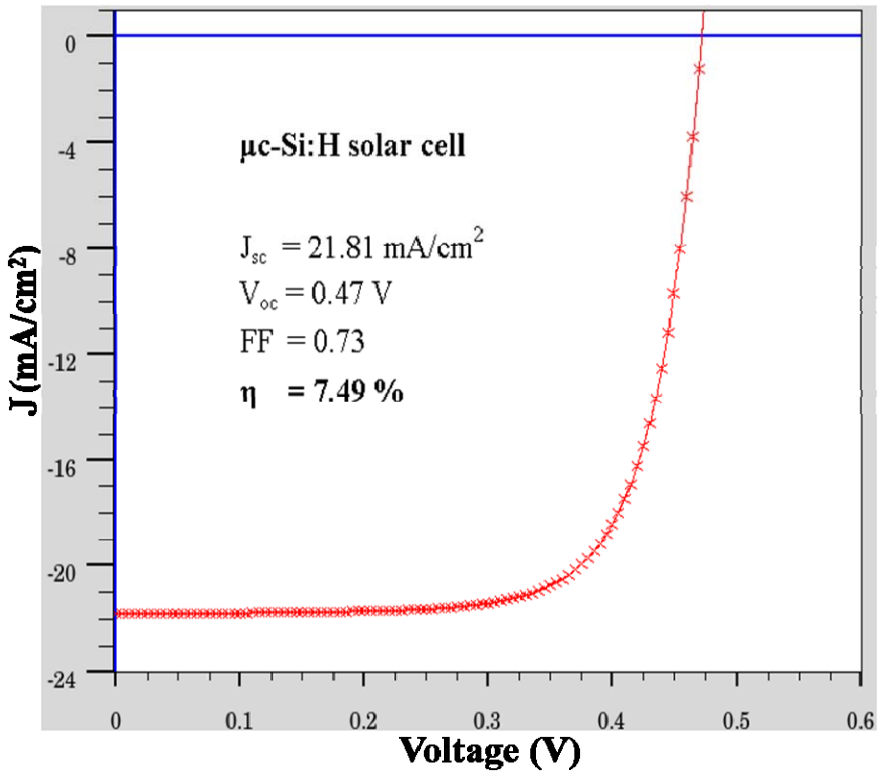

Fig. 4-8 The illuminated J-V characteristic curve of µc-Si:H p-i-n solar cell

Table 4-3 The electrical characteristics for a-Si:H and µc-Si:H solar cells.

Description	J_{sc} (mA/cm^2)	V_{oc} (V)	FF	Efficiency (%)
a-Si:H solar cell	13.3	0.83	0.74	8.37
µc-Si:H solar cell	21.81	0.47	0.73	7.49

4.3 Tandem Solar Cell with and without x Layer

The Tandem solar cell is constituted by the optical and electrical series connection of an amorphous silicon (a-Si:H) top cell and a microcrystalline silicon (μc-Si:H) bottom cell. As a consequence of the electrical series connection, the short-circuit current density J_{sc} of the whole tandem is limited by the absorber (top or bottom cell) with the lower current generation capabilities. The thickness of the a-Si:H intrinsic layer must be made as thin as possible to minimize the Staebler-Wronski effect. It is generally thin (about 250 nm) in order to collect a maximum of the photo-induced electrons. The μc-Si:H intrinsic layer has to be thicker (about 2 μm) because of its indirect band-gap and the necessity to match the photo-current generated by the two stacked cells.

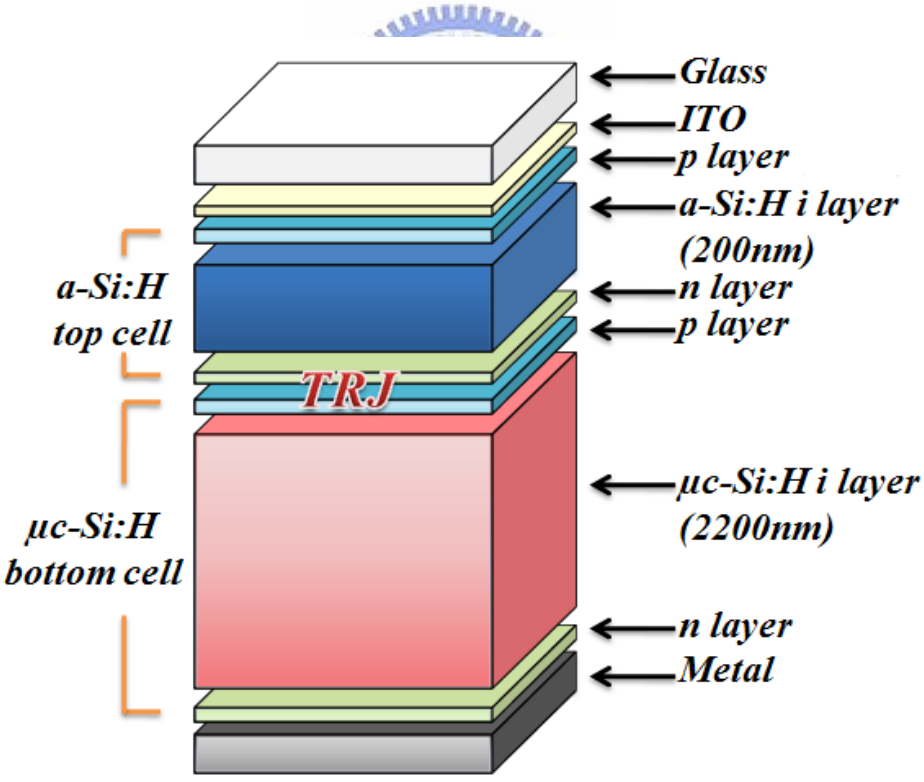

Fig. 4-9 Tandem solar cell without x layer.

Tandem solar cell with the following structure as shown in **Fig. 4-9** was used in the simulations: flat glass / ITO / p-a-SiC:H / i-a-Si:H($d_{i,top}$) / n-a-Si:H / p-μc-Si:H /

i-μc-Si:H($d_{i,bot}$) / n-a-Si:H / Ag. The Ag forms the BR. The absorber layers were relatively thin ($d_{i,top}$ 200 nm and $d_{i,bot}$ 2.2μm), and no interlayer was applied. The calibrated optical and electrical parameters of undoped, doped a-Si:H and μc-Si:H layers were used in the simulations.

4.3.1 Simulation Model

Since the tandem cell was fabricated under the same conditions as the single-junction cells we used this set of parameters for modeling of the tandem cells. Also, The physical models we used here are identical with a-Si:H and μc-Si:H solar cell as mentioned before except thickness.

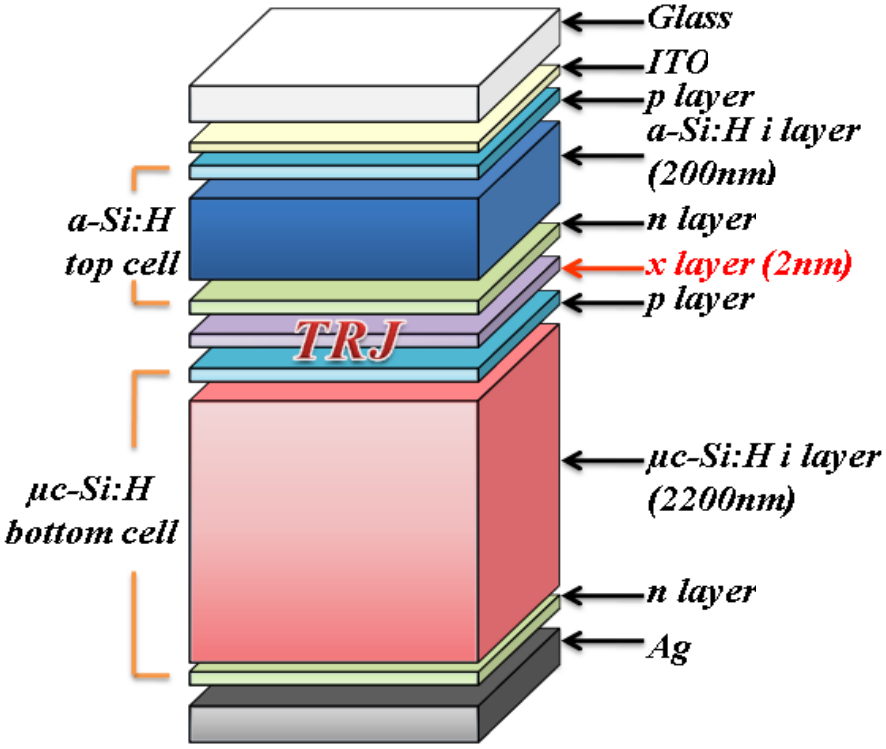

Fig. 4-10 Tandem solar cell with x layer.

The physics controlling the electric transport in n-a-Si:H and p-μc-Si:H interface is generally called tunneling recombination junction (TRJ) as shown in **Fig. 4-9** which is

explored with atlas. When modeling the tandem cell as a complete stacked structure (pinpin device), and not using a x layer for the TRJ between the two-component cells, we could not obtain an realistic J-V curve for illuminated tandem cell unless adding a strong-recombination layer (which we call an x-layer) sandwiched between the n- and p-layers of the two inter-cell contact regions as shown in **Fig. 4-10**. We also have found that the parameters of the TRJ, such as doping concentration and the defect density in the doped layers of the TRJ, must be optimized in order to get the realistic illuminated characteristics of the tandem cell. The parameters for models, such as the mobility gap and the defect density of the x-layer, were also sensitive for obtaining the realistic tandem cell characteristics. After determining the parameters of the TRJ models, we obtained an excellent J-V curve of tandem cell with added-x-layer models. A typical J-V curves for both cases (with and without x layer) are shown in **Fig. 4-11**.

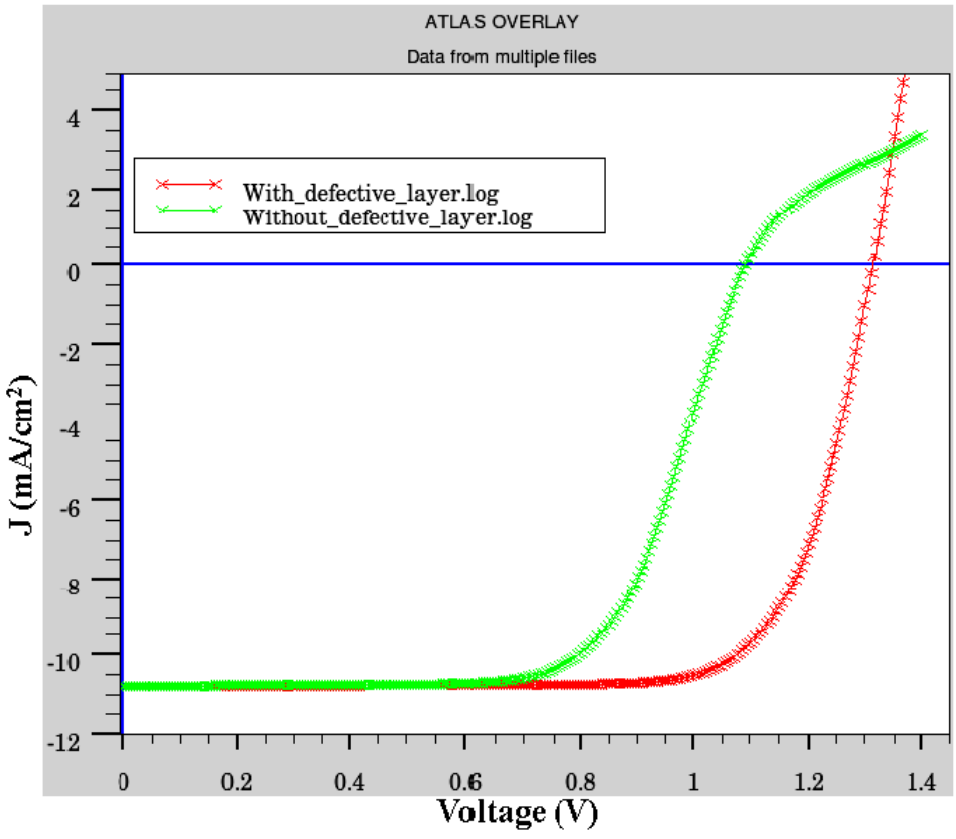

Fig. 4-11 The J-V curves of tandem solar cells with and without x layer.

The parameters which were used to describe TRJ are reported in **Table 4-4** and **Fig. 4-12** shows the energy band diagram of the tandem cell in thermal equilibrium for insertion of special layers (x-layer) in the tunnel/recombination junction on tandem cells. **Fig. 4-13** shows (a) the distribution of hole current density, (b) electron current density and (c) the recombination rate in the cell. In the cell carrier's current density increases as the carriers move toward the "tunnel junctions". But at "tunnel junction" the hole current is seen to drop very low in the n region, while correspondingly the electron current is seen to drop very low in the p region. This indicates a very strong recombination process is happening in the "tunnel junction" which manifests itself in the Fig. 3c, the plot of recombination rate in the contacts. This good recombination in contacts is needed for continuity of currents. Careful examination of **Fig. 4-13(b)** shows that there actually is a small component of electron current in the second sub-cell moving toward the first "tunnel junction", which is due to the unbalance of the net photo-carrier generation. Hence, the modeling shows the delicate balancing going on at these contacts [28]. The crucial role of recombination in the "tunnel junction" contacts of multi-junction solar cells is very different than the physics in the true tunnel junctions of tunneling diodes, in which electrons tunnel through the band gap from valence band to conduction band. Here electrons must fall from the conduction band to the valence band through a recombination process and fill in holes. Because the electrical field in the "tunneling junction" is so strong due to our wanting to dope heavily to increase the field across the absorbers and because of this field's orientation (see **Fig. 4-12**), it acts against the holes and the electrons moving into the x-layers in contact region. Hence, our modeling shows that supplying carriers to this recombination can be a problem. It is in this supply role that tunneling is needed through the n-layer for electrons to supply the x-layer and through p-layer for holes to supply the x- layer. The key process in the functioning of the contact region is recombination. Any material layer that enhances this recombination will reduce the dipole modification and will enhance cell performance if it does not strongly absorb light.

Hence, the TRJ region cannot be represented with a resistor or diode model, and such a layer could have the state distribution properties of a metal, a narrow gap semiconductor, or a very heavily defective semiconductor [28].

Table 4-4 TRJ (a-Si:H n-layer, x layer, μc-Si:H p-layer) parameters.

Parameter	n-a-Si:H	x	p-μc-Si:H
Layer thickness (nm)	10~30	1~5	10~30
Mobility gap (eV)	1.8	1.1	1.3
Donor doping density (cm-3)	$9x10^{18}$		
Acceptor doping density (cm-3)			$1x10^{19}$
Electron mobility(cm2/Vs)	20	0.1	100
Hole mobility(cm2/Vs)	4	0.1	25
Electron life time (μs)	0.01	0.01	0.01
Hole life time (μs)	0.1	0.1	0.1
Effective DOS in the valance and conduction bands (cm^{-3})	$2x10^{20}$	$2x10^{20}$	$2x10^{20}$
Exponential tail Prefactors NTD, NTA ($cm^{-3}eV^{-1}$)	$4x10^{21}$	$4x10^{21}$	$4x10^{21}$
Characteristic energy WTD (VB tail) (eV)	0.05	0.05	0.02
Characteristic energy WTA (CB tail) (eV)	0.03	0.03	0.01
Gaussian distribution density NGD, NGA ($cm^{-3}eV^{-1}$)	$9x10^{18}$	$1x10^{19}$	$5x10^{18}$
Characteristic energy for Gaussian distribution WTD (donor like state) (eV)	0.2	0.2	0.2
Characteristic energy for Gaussian distribution WTA (acceptor like state) (eV)	0.2	0.2	0.2
Peak of donor like Gaussian distribution EGD (meas. From Valance edge) (eV)	0.78	0.59	0.4
Peak of acceptor like Gaussian distribution EGA(meas. From Conduc. edge) (eV)	0.52	0.16	0.6
Correlation energy U (eV)	0.5	0.35	0.3

[a] measured from the conduction band edge ; [b] measured from the valance band edge, x is tunnel recombination layer.

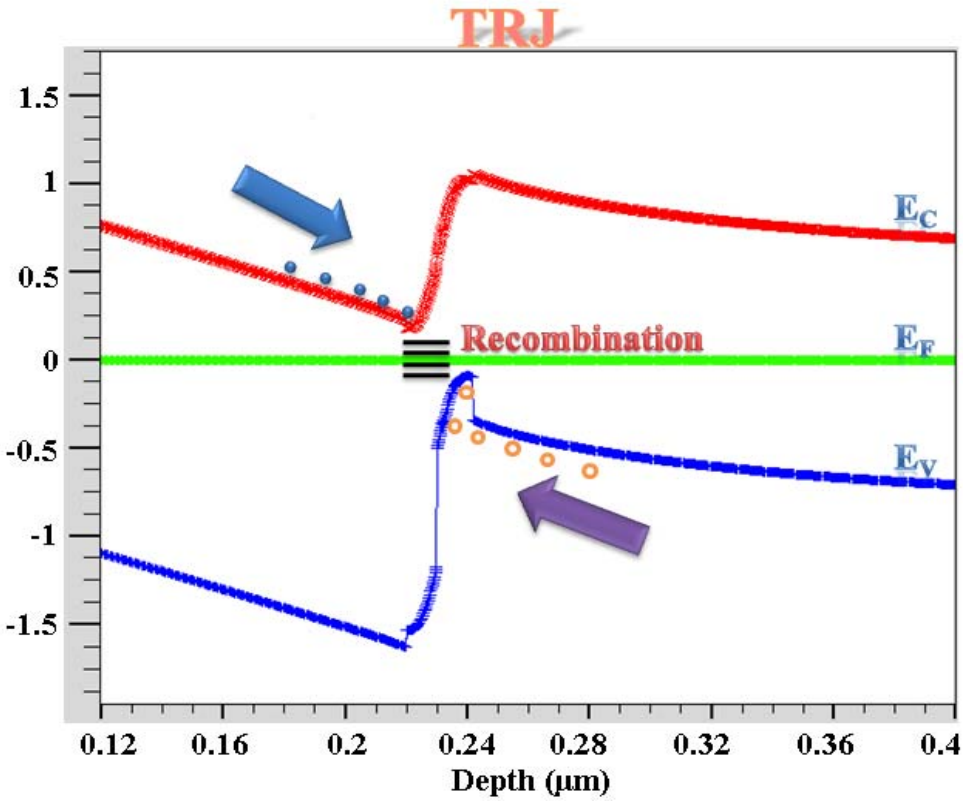

Fig. 4-12 The added-x layer TRJ (tunneling recombination junction) band diagram. The strategy is to simulate the tunneling effect around x region in band gap.

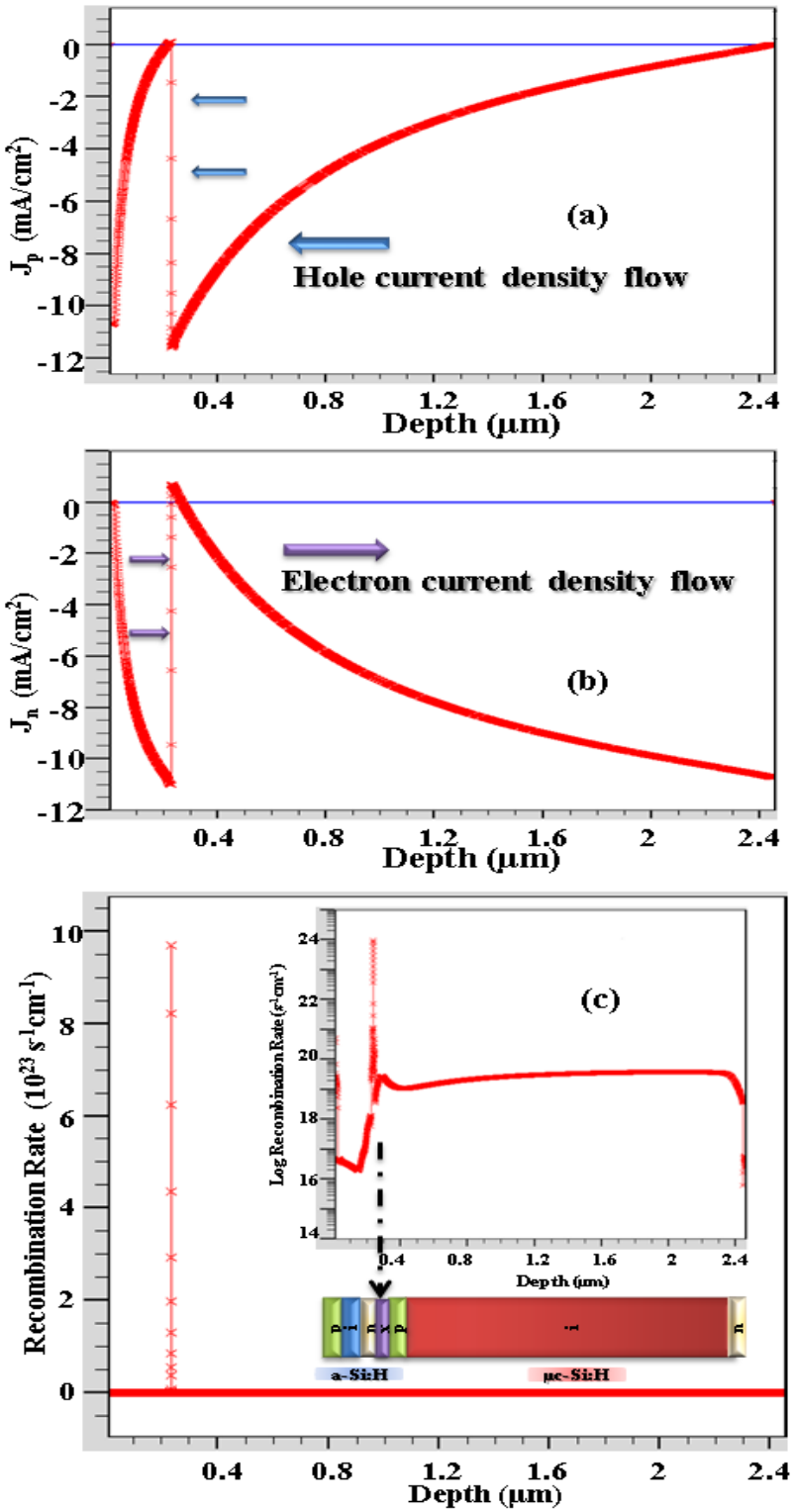

Fig. 4-13 Charge transport in tandem cells under AM1.5G illumination conditions.

(a) Hole current density distribution;

(b) Electron current density distribution;

(c) Recombination rate distribution.

4.4 The Effect of the Bandgap in Bottom Cell on the Solar Cell Performance

4.4.1 Influence of i-Layer Bandgap on Single-Junction Cell Performance

Here we simulate the single-junction solar cell performance with altering the band gap and tail distribution of i-layer. **Table 4-5** shows the tail distribution (WTA, WTD) of i-layer is broader as the E_g increases. **Fig. 4-15** sketches the J-V curve and **Fig. 4-14** shows the optimal E_g of i-layer for single-junction cell is 1.4 eV, and the J_{sc}, F.F., Eff. are optimized except V_{oc}.

Table 4-5 Simulation results for μc-Si:H solar cell with different E_g of i layers.

Eg (eV)	WTA (eV)	WTD (eV)	Voc (V)	Jsc (mA/cm^2)	F.F.	Eff.(%)
1.1	0.005	0.01	0.303	21.58	60.75	3.97
1.2	0.01	0.02	0.38	21.65	65.1	5.38
1.3	0.02	0.04	0.4347	21.74	71.29	6.74
1.4	0.03	0.05	0.5	21.81	73	7.98
1.5	0.04	0.07	0.53	20.13	69.18	7.41
1.6	0.05	0.08	0.558	18.56	70.12	7.26

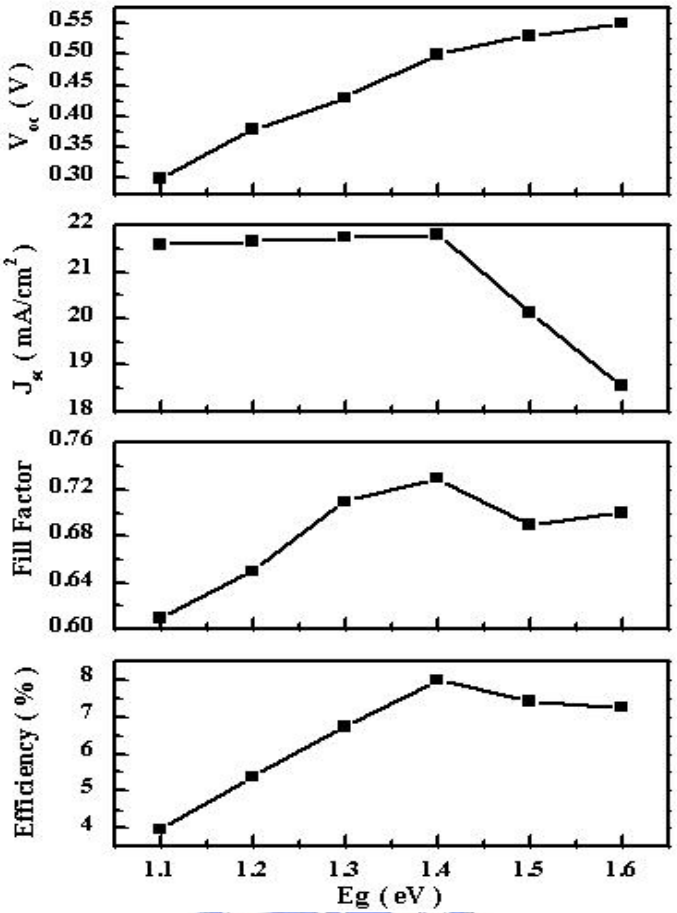

Fig. 4-14 Photovoltaic performances of single-junction cells with different E_g of i layers

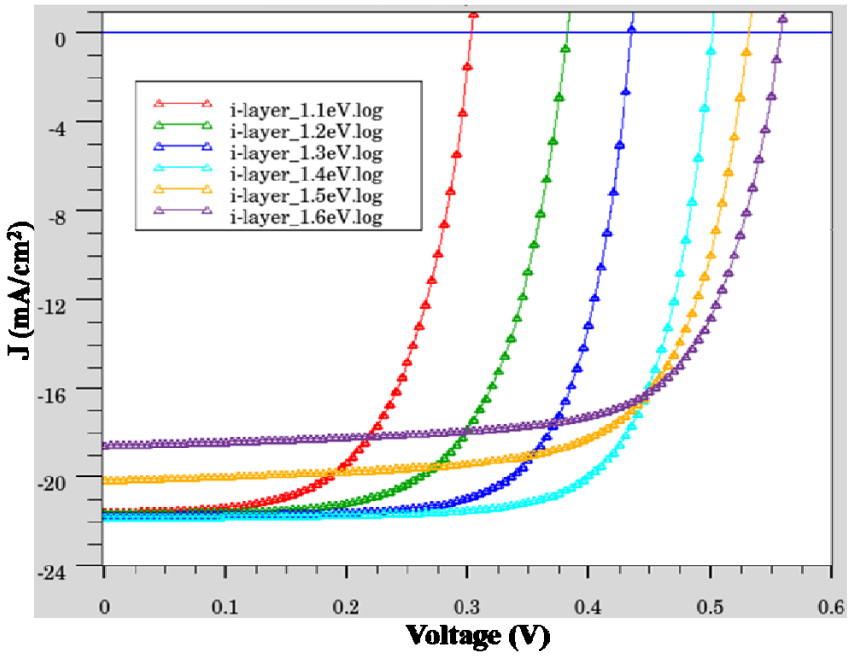

Fig.4-15 The J-V curves of single-junction cells with varied E_g of i-layers

4.4.2 Influence of Bottom Cell Bandgap on Tandem Cell Performance

Tandem solar cell consists in a multi-junction cell with a top-cell and a bottom-cell. As the **Fig. 4-16** shown, the optimal E_g of i-layer for Tandem solar cell is 1.4 eV which is identical with the single-junction solar cell. The open circuit voltage (V_{oc}) increases with the E_g, but the short circuit current (J_{sc}) decreases after the 1.4 eV of the E_g because the tail distribution of DOS is broader and broader with E_g (**Table 4-6**) which results in the reducing of short circuit current (J_{sc}). The optimal value of F.F. is also located at 1.4 eV. As a whole, the performance of tandem solar cell is optimized at 1.4 eV of bottom cell. This phenomenon also can be observed in **Fig. 4-17**. The lower E_g makes the efficiency decease a lot, although the J_{sc} keeps high value. In general, the E_g keeps around 1.4 eV is good for whole device. And comparing the highest and lowest E_g, the former get the better performance. It means the E_g of bottom cell shouldn't be too low (<1.3eV) to avoid the efficiency decline. In conclusion, The best E_g of the bottom cell is about 1.4 eV for tandem solar cells.

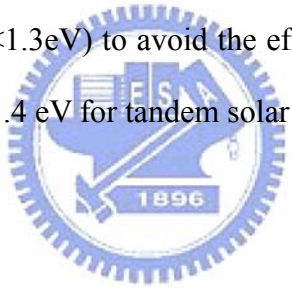

Table 4-6 Simulation results for tandem solar cell with varied E_g of bottom cell.

Eg (eV)	WTA (eV)	WTD (eV)	Voc (V)	Jsc (mA/cm^2)	F.F.	Eff.(%)
1.1	0.005	0.01	1.13	10.78	71.8	8.78
1.2	0.01	0.02	1.21	10.78	72.6	9.49
1.3	0.02	0.04	1.27	10.78	74	10.24
1.4	0.03	0.05	1.31	10.78	74	10.75
1.5	0.04	0.07	1.32	10.64	71.3	10.01
1.6	0.05	0.08	1.33	9.61	73	9.43

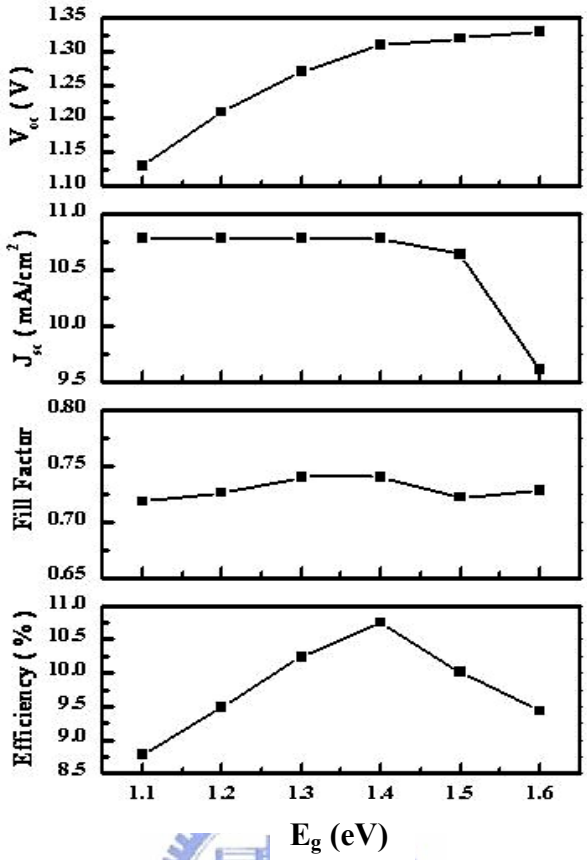

Fig. 4-16 Photovoltaic performances of tandem solar cell with varied E_g of bottom cell.

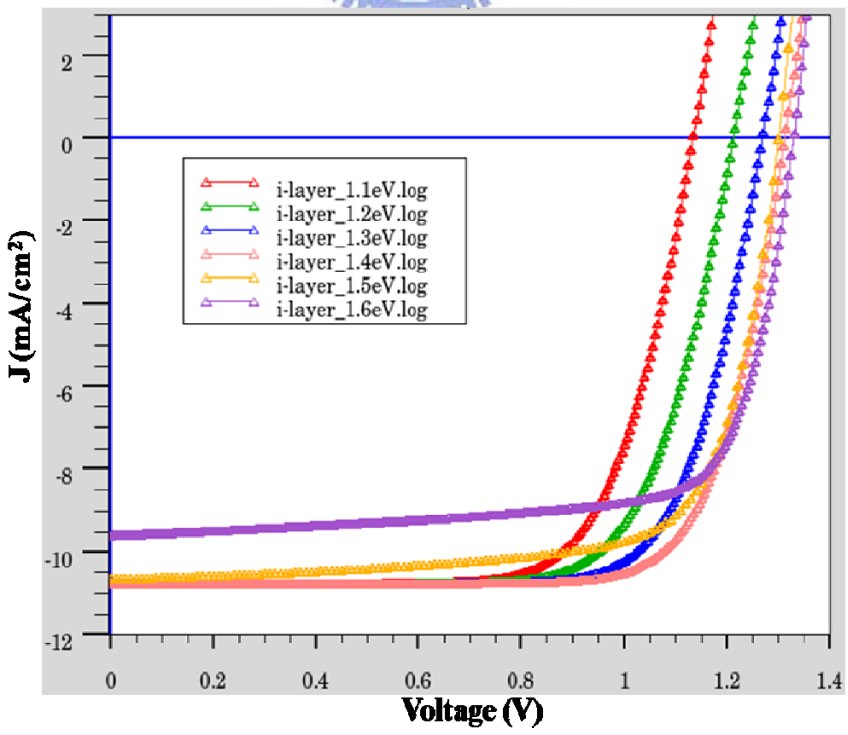

Fig. 4-17 The J-V curves of tandem solar cells with varied E_g of bottom cell.

4.5 Deposition techniques for microcrystalline silicon

As microcrystalline silicon cells do not show any light-induced degradation effect, this material can be considered to be an interesting substitute for low-bandgap amorphous silicon-germanium alloys based on the use of germane (an expensive source gas). For this reason, broad research has been started on microcrystalline silicon solar cells. Here we deposit the μc-Si:H film by plasma-enhanced chemical vapor deposition (PECVD) and alter the conditions for studying on crystallinity (X_c) of μc-Si:H film. Finally the 50% of crystallinity is achieved by H_2 dilution skill.

4.5.1 Effect of H_2 Dilution on Crystallinity

Fig. 4-18 shows the crystallnity of μc-Si:H films with H_2 dilution of 800, 1100, 1350, 1700, 2000 sccm. In surface growth models one considers that μc-Si:H nucleation is due to enhanced surface diffusion of SiH_3 radicals due to the coverage of the surface by hydrogen [15].

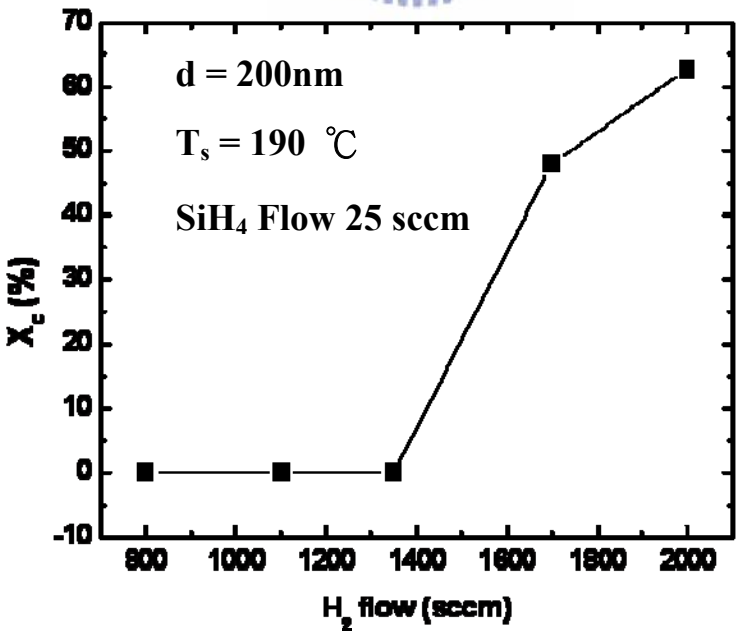

Fig. 4-18 The crystallinity of μc-Si:H increases with H_2 flow.

This enhaced surface mobility would then promote the incorporation of silicon into sites of minimum energy and form stable crystallites. Moreover, selective etching of the amorphous phase by atomic hydrogen have also been considered. When the H_2 flow increase , those effects have mentioned will be more distinct. In summary, the crystallinity of μc-Si:H increases with H_2 flow.

4.5.2 Effect of rf Power on Crystallinity

The growth of μc-Si:H is affected by rf power. Silicon ions of high energy as the increase of the deposition rate is achieved by the increase of the rf power. The contribution of clusters and nanocrystals can be avoided as long as the secondary reactions are kept below some threshold. Thus, besides simplifying the plasma chemistry, the combination of a high power plasma with a high density of atomic hydrogen as required for crystallization (**Fig. 4-19**).

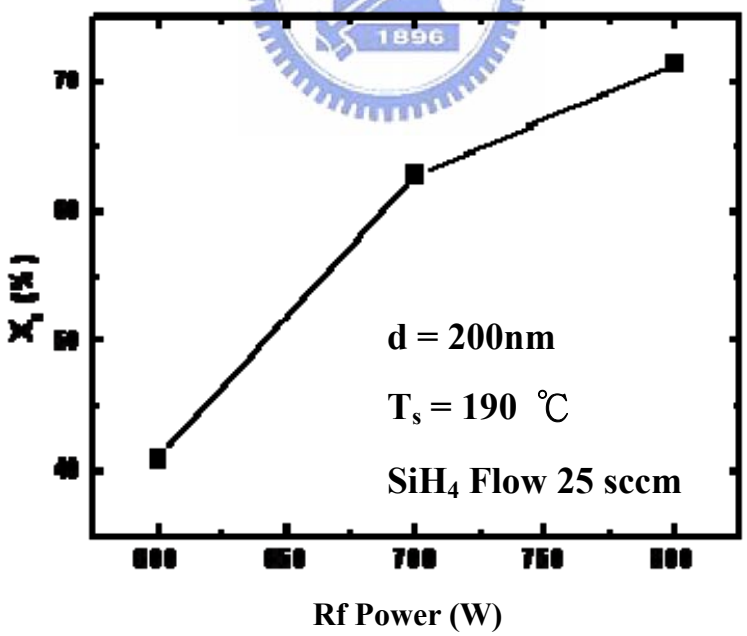

Fig. 4-19 The crystallinity of μc-Si:H increases with rf Power

But high rf power cause the ion bombardment on the surface which ruin the p/i interface in particularly. The very high frequency (between 30 and 300 MHz) rf power leads to a softer

ion bombardment, which is more favorable to microcrystalline Si formation, and, at the same time, allows relatively high growth rates.

4.5.3 Effect of Total Gas Flow

We set three basic total flows F_0 (H_2+SiH_4) which represent triangle, circle, and square symbols. F represent the realistic total flow. The Relative total gas flow is defined by (F/F_0) that means normalization and the SiH_4 flow keeps 25 sccm in whole process. In **Fig. 4-20**, the deposition rate increase with relative total gas flow (F/F_0). It means when the total injecting gas flow increases, the gas reaction will be more drastic which makes the deposition rate increase, too. Deposition rate increases as H_2/SiH_4 decreases can be also observed on three symbols.

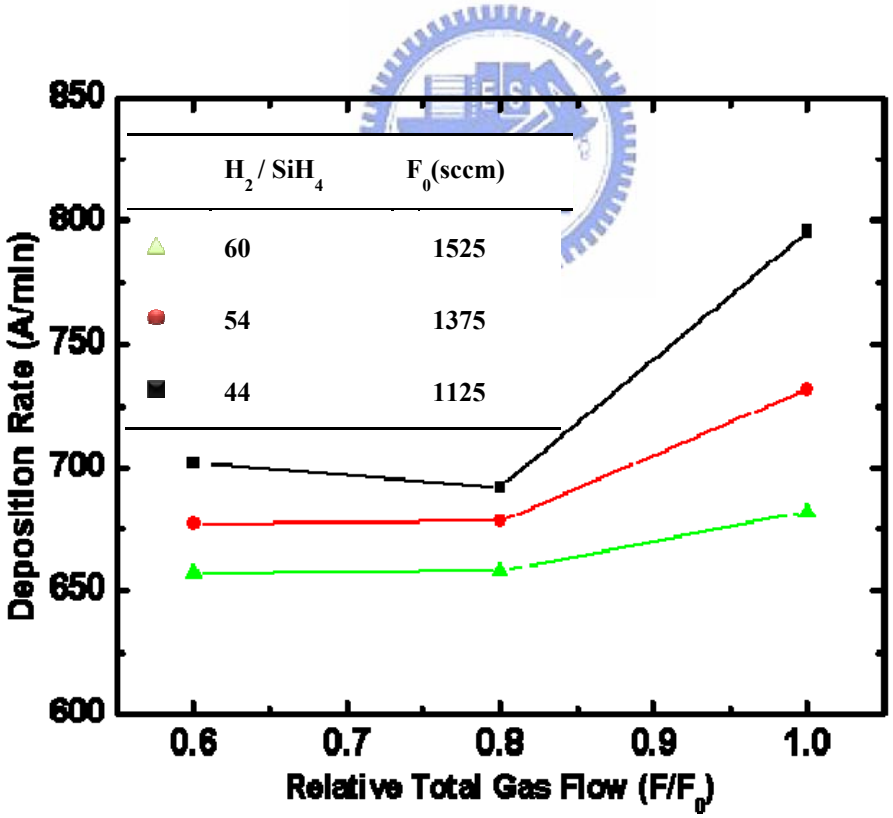

Fig. 4-20 Deposition rate vs. relative total gas flow (F / F_0).

On the other side, crystallinity decreases as (F/F_0) increases which has shown in **Fig. 4-21.** The crystallinity decreases with H_2 / SiH_4 because the selective etching effect of H atom. Both amorphous and microcrystalline silicon are deposited and etched simultaneously, but with an etching rate much higher for the amorphous phase, hence increasing the crystalline volume fraction of the growingfilm. In conclusion, the relative total gas flow increase with the deposition rate but makes the crystallinity decreases. The increasing H_2 flow enhances the etching effect of H atom, therefore the crystallinity increases.

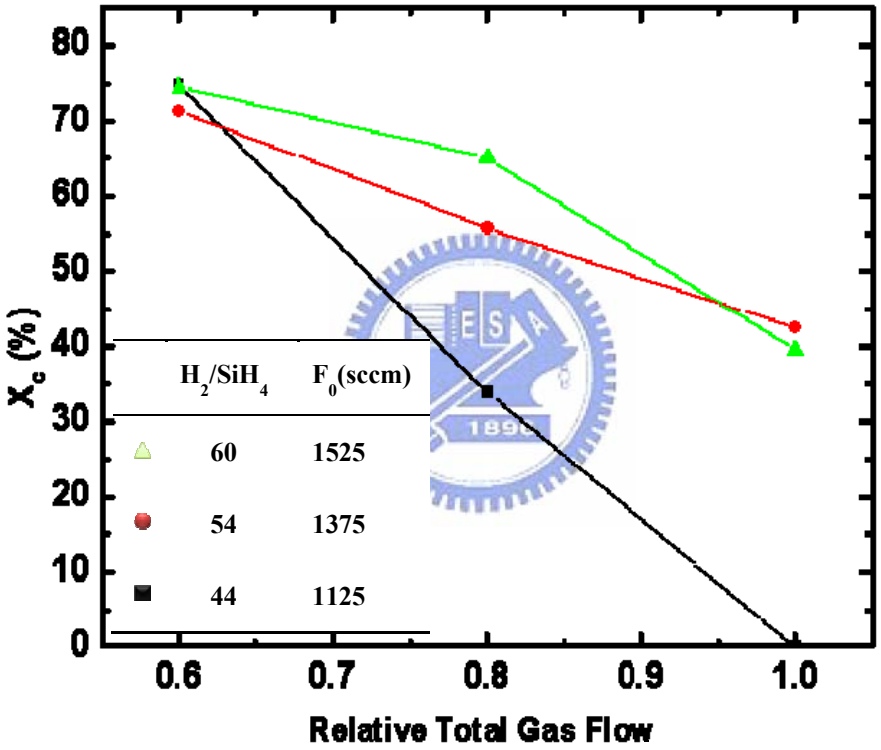

Fig. 4-21 Crystallinity vs. relative total gas flow (F / F_0)

4.5.4 Crystallinity vs. modulating the H_2 flow percentage of next layer

In order to maintain the crystallinity of whole film, we modulate the H_2 flow by decreasing the flow with four layers in series and the total thickness is 1500 nm. The symbol Z represent that the next layer H_2 is divided by present H_2 flow. We set the H_2 flow in first layer to be 710 sccm and the substrate is glass. As the **Fig. 4-22** shown, although the

crystallinity increases with the Z, the crystallinity is still too high..

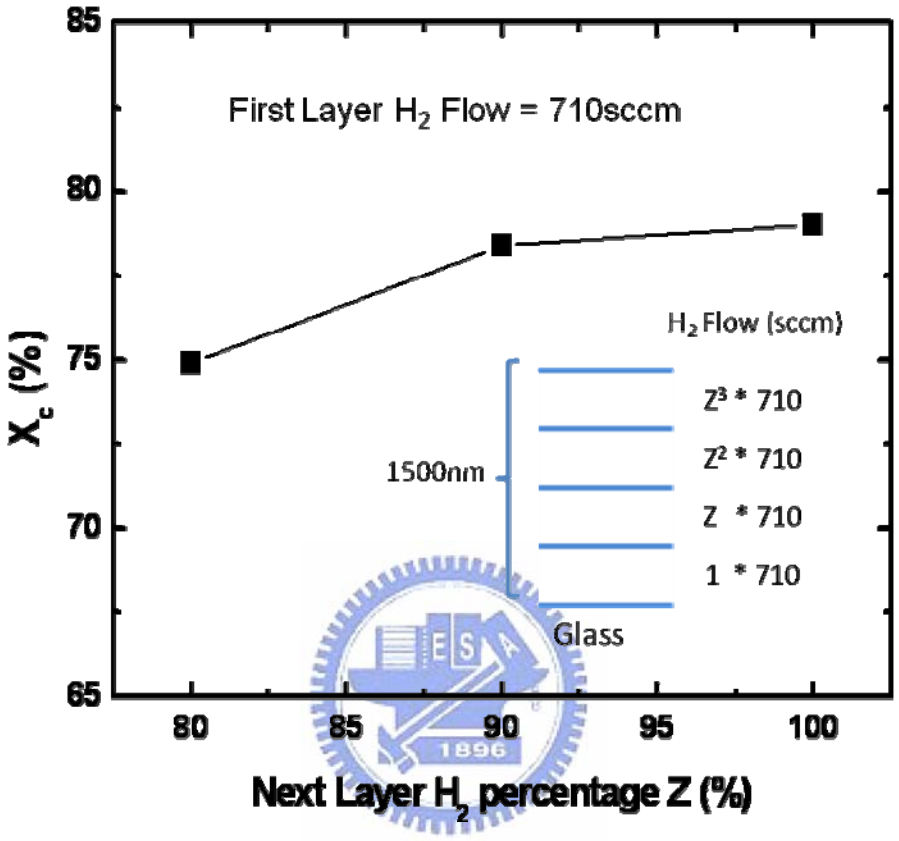

Fig. 4-22 Crystallinity vs. next layer H_2 flow percentage Z

4.5.5 Crystallinity vs. modulating the initial H_2 flow

In last section, we modulate the H_2 flow ratio each layer but the crystallinity of whole film is still high. Thus we vary the initial H_2 flow (F_0) and maintain the deceasing ratio each layer (Z) to be 80%. The total thickness of film is 400nm and the substrate is glass. As the **Fig. 4-23** shown, the initial H_2 flow influence the crystallinity drastically. When the initial H_2 flow (F_0) is 600 sccm, the crystllinity of the film is about 55%. In brief, the incubation layer is very crucial for the crystallinity of the film, and controlling the initial condition of deposition is worth studying.

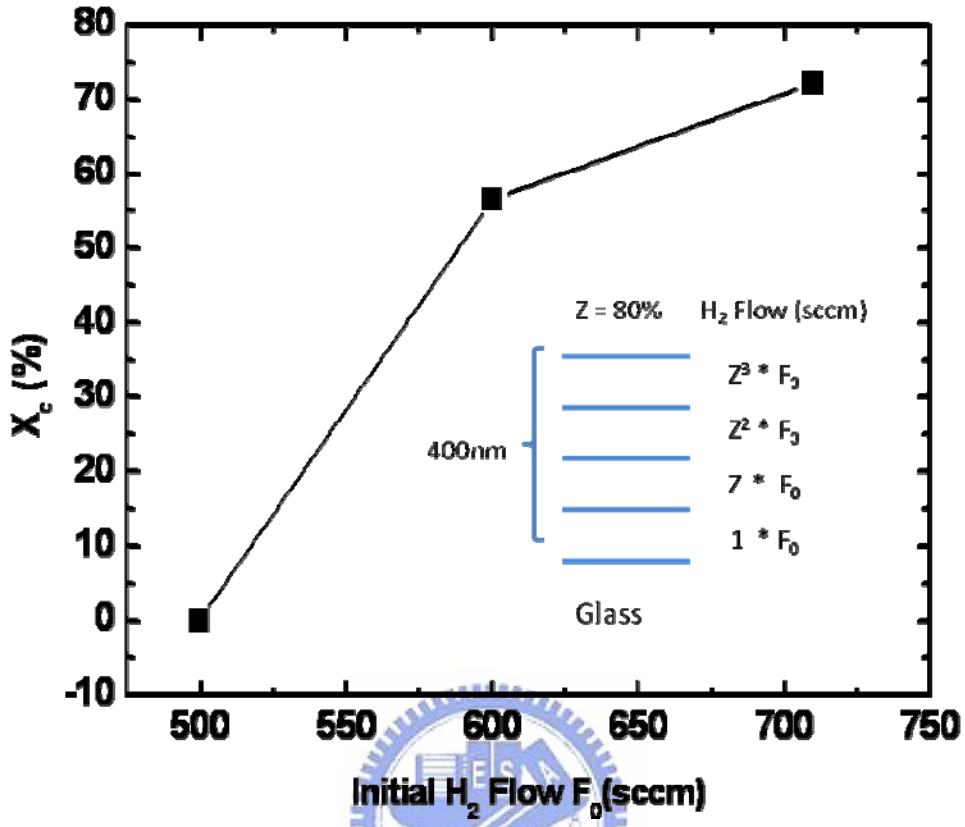

Fig. 4-23 Crystallinity vs. initial H_2 flow F_0

4.5.6 Effect of varied SiH_4 flow rate of three substrates on crystallinity of μc-Si:H film

We are curious about the effect of varying substrate on μc-Si:H film, thus using three different substrates, glass, glass/a-Si:H, Asahi U/a-Si:H to study the effect of substrate on crystallinity of μc-Si:H film. The H_2 flow, thickness of each layer, and total thickness have shown in **Fig. 4-24**. The **Fig. 4-25** shows the crystallinity is lowest when the substrate is Glass and crystallinity decreases as SiH_4 increases. We consider that a-Si:H is the key for crystallinity decreasing. In conclusion, the initial conditions of deposition can almost control the crystallinity of whole μc-Si:H film and the crystallinity of μc-Si:H film about 50% is also achieved.

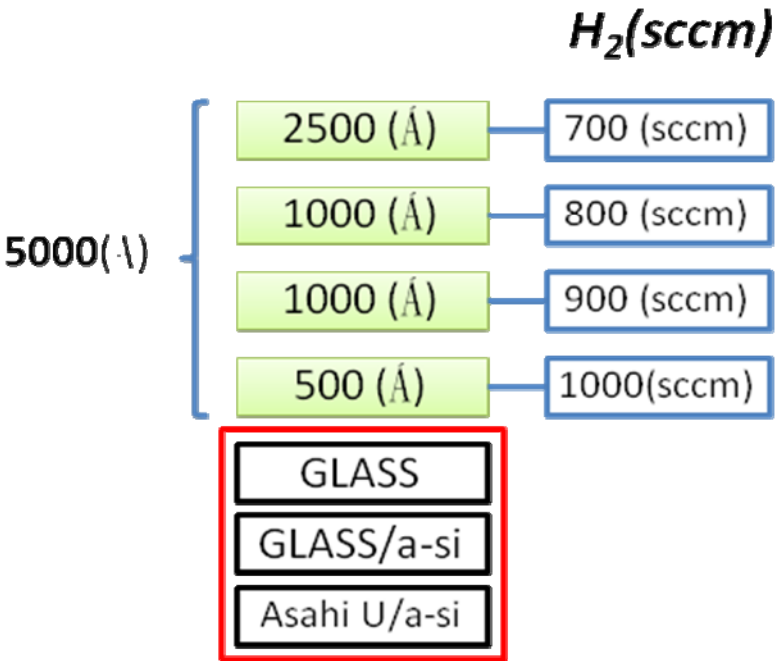

Fig. 4-24 The deposited parameters of μc-Si:H film.

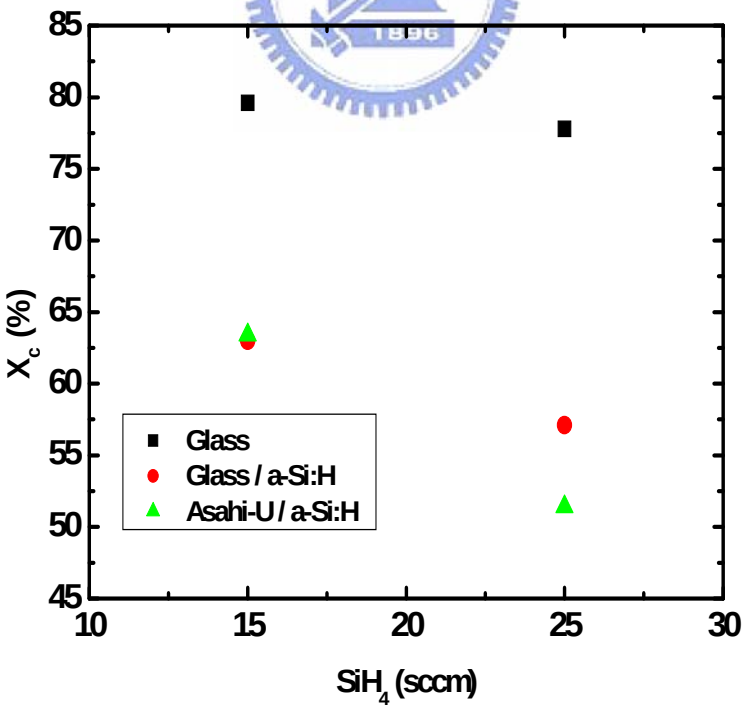

Fig. 4-25 Crystallinity with different SiH_4 flow rate on three different substrates.

Chapter 5

Conclusions

In this study, computer modeling with the Atlas program is used as a new approach for obtaining optimal performance of the solar cell. Increasing the dangling bond density from $5x10^{15}cm^{-3}$ to $5x10^{18}cm^{-3}$ in a-Si:H i-layer, the solar cell efficiency decreased from 8.37% to 5.91%. The increase in the dangling bond density increases the amount of the recombination centers and recombination capability. These defects may be caused by light illumination which plays a major role in the degradation of a-Si:H solar cells.

The crucial point for tandem solar cell is the insertion of a special layer (x-layer) between individual cells. The simulation results showed a drastically drop of electron and hole current in p and n layers, respectively. This indicates a very strong recombination process occurred in the TRJ. The tunneling is needed through the n-layer for electrons to supply the x-layer and through p-layer for holes to supply the x- layer. The key process in TRJ is recombination.

Tandem solar cell performance was simulated by altering the bottom cell bandgap (E_g) and the tail state distribution. The spatial disorder in the atomic structure results in the localized states within the mobility gap strongly influence the electron transition. Thus, when tail state distribution of DOS becomes broader with increasing E_g, the region of carrier confinement expands which leads the reduction of J_{sc} in the cell. The open circuit voltage (V_{oc}) increases with E_g, but the short circuit current (J_{sc}) decreases as the bandgap lower than 1.4 eV. Combining the effects of V_{oc} and J_{sc}, the efficiency increases from 8.78% to 10.78%, and then decline to 9.43% with the increase of bandgap. Considering the value of E_g, the higher E_g gets a better performance. The results in the study showed the E_g of bottom cell should not be lower than 1.3eV to avoid the efficiency decline.

In realistic deposition process we deposited the μc-Si:H film by plasma-enhanced

chemical vapor deposition (PECVD). H_2 flow rate, rf power and grading H_2 flow rate were used to control the crystallinity. In this study we have found that the initial H_2 flow rate and substrate surface strongly influence the crystallinity of μc-Si:H. The initial deposition condition determined the crystallinity of the whole μc-Si:H film. The crystallinity would drop sharply when amorphous silicon was deposited on glass and used as substrate. Finally crystallinity of about 50% was achieved by modulating H_2 flow.

Reference

[1] Investigation M.A. Green, K. Emery, Y. Hisikawa, and W. Warta, "*Solar cell efficiency tables*", Prog. Photovoltaics: Res. Appl., **15**, 425 (2007).

[2] Investigation A. Shah, J. Meier, A. Buechel, U. Kroll, J. Steinhauser, F. Meillaud, H.Schade, and D. Dominé, "*Towards very low-cost mass production of thin film Si PV solar modules on glass*", Thin Solid Films, **502**, 292 (2006).

[3] SILVACO, Data Systmes Inc., Santa Clara, CA: http://www.silvaco.com/products/device_simulation/atlas.html

[4] Jef Poortmans and Vladimir Arkhipov, "*Thin Film Solar Cells Fabrication,Characterization and Application*", (Wiley Series in Materials for Electronic and Optoelectronic Applications, 2006).

[5] D. L. Staebler and C. R. Wronski, "*Reversible conductivity changes in discharge-producedamorphous Si*", Appl. Phys. Lett., **31**, 292 (1977).

[6] Spear WE, Lecomber PG., "*Electronic properties of substitutionnally doped amorphous Si and Ge*", *Phil. Mag.*, **33**, 935 (1976).

[7] M. Vanecek and A. Poruba, "*Fourier-transform photocurrent spectroscopy of microcrystalline silicon for solar cells*", Appl. Phys. Lett., **80**, 719 (2002).

[8] F. Meillaud, E. Vallat-Sauvain, X. Niquille, et al., "*Light-induced degradation of thin film amorphous and microcrystalline silicon solar cells*", in Proceedings of the 31st IEEE Photovoltaic Specialists Conference, pp. 1412, Lake Buena Vista, Fla, USA, January 2005.

[9] B. Yan, G. Yue, J. Owens, J. Yang, and S. Guha,"*Light-induced metastability in hydrogenated nanocrystalline silicon solar cells*", Appl. Phys. Lett., **85**, 1925 (2004).

[10] A. V. Shah, H. Schade, M. Vanecek, J. Meier Prog.,"*Thin-film Silicon Solar Cell Technology*", Prog. Photovolt: Res. Appl., **12**, 113 (2004)

[11] A. Shah, J. Meier, E. Vallat-Sauvain, C. Droz, U. Kroll, N. Wyrsch, J. Guillet, and U. Graf,"*Microcrystalline silicon and 'micromorph' tandem solar cells*", Thin Solid Films, **403-404**, 179 (2002).

[12] O. Vetterl, F. Finger, R. Carius, P. Hapke, L. Houben, O. Kluth, A. Lambertz, A. Mück, B. Rech, and H. Wagner,"*Intrinsic microcrystalline silicon: A new material for photovoltaics*", Sol. En. Mat. Sol. Cells, **62**, 97 (2000).

[13] Investigation A. Matsuda,"*Growth mechanism of microcrystalline silicon obtained from reactive plamsas*", Thin Solid Films, **337**, 1 (1999).

[14] Investigation J. Robertson,"*Growth mechanism of hydrogenated amorphous silicon*", J. Non-Cryst. Solids, **266-269**, 79 (2000).

[15] Investigation A. Matsuda, "*Microcrystalline silicon: Growth and device application*", J. Non-Cryst. Solids, **338-340**, 1 (2004).

[16] Investigation R. Terasa, M. Albert, H. Grüger, A. Haiduk, and A. Kottwitz, "*Investigation of growth mechanisms of microcrystalline silicon in the very high frequency range*", J. Non-Cryst. Solids, **266-269**, 95 (2000).

[17] Investigation R.C. van Oort, M.J. Geerts, J.C. van den Heuvel, and J.W. Metselaar, "*Hydrogen plasma etching of amorphous and microcrystalline silicon*", Electronic Lett., **23**(18), 967 (1987).

[18] Investigation C.C. Tsai, G.B. Anderson, R. Thompson, and B. Wacker, "*Control of silicon network structure in plasma deposition*", J. Non-Cryst. Solids, **114**, 151 (1989).

[19] Investigation K. Nakamura, K. Yoshida, S. Takeoka, and I. Shimizu, "*Roles of atomic hydrogen in chemical annealing*", Jpn. J. Appl. Phys., **34**, 442 (1995).

[20] Investigation R.L. McCreery, "*Chemical Analysis*", in *Raman spectroscopy for chemical analysis*, **157**, Wiley (2000).

[21] E.I. Terukov et al. "*The influence of deposition parameters on the structure of nanocrystalline silicon*", Materials Science and Engineering, **69-70**, 266 (2000).

[22] Poissant, Chatterjee, and Roca i Cabarrocas"*Analysis and optimization of the performance of polymorphous silicon solar cells: Experimental characterization and computer modeling*", J. Appl. Phys. **94**, 7305 (2003)

[23] A.J. Letha, H.L. Hwang "*Two-dimensional modelling and simulation of hydrogenated amorphous silicon p+–n–n+ solar cell*", Journal of Non-Crystalline Solids, **355**, 148 (2009).

[24] S. Hamma, P. Roca i Cabarrocas, "*Determination of the mobility gap of microcrystalline silicon and of the band discontinuities at the amorphous/microcrystalline silicon interface using in situ Kelvin probe technique*", Appl. Phys. Lett., **74**, 3218 (1999)

[25] T. Merdzhanova, R. Carius, S. Klein, F. Finger, D. Dimova-Malinovska, "*Photoluminescence energy and open circuit voltage in microcrystalline silicon solar cells*", Thin Solid Film, **285**, 451 (2004).

[26] Madhumita Nath, P. Roca i Cabarrocas, "*The open-circuit voltage in microcrystalline silicon solar cells of different degrees of crystallinity*", Thin Solid Films, **516**, 6974 (2008).

[27] X. Han et al., "*Stability of microcrystalline silicon materials under light soaking*", Materials Science in Semiconductor Processing , **9**, 300 (2006).

[28] J.Y. Hou, J.K. Arch, S.J. Fonash, S. Wiedeman and M. Bennel, "*An Examination of the "Tunnel junctions" in triple junction a-Si:H based solar cells : modeling and effects on performance*", IEEE 22nd PVSEC, 1260, Las Vegas 1991.